

UC Berkeley

UC Berkeley Electronic Theses and Dissertations

Title

Regulation of listeriolysin O translation and c-di-AMP stress response in *Listeria monocytogenes*

Permalink

<https://escholarship.org/uc/item/88k557jj>

Author

Peterson, Bret Nicholas

Publication Date

2019

Peer reviewed|Thesis/dissertation

Regulation of listeriolysin O translation and c-di-AMP stress response in *Listeria monocytogenes*

By

Bret Nicholas Peterson

A dissertation submitted in partial satisfaction of the

requirement for the degree of

Doctor of Philosophy

in

Microbiology

in the

Graduate Division

of the

University of California, Berkeley

Committee in Charge:

Professor Daniel A. Portnoy, Chair

Professor Russell E. Vance

Professor Daniel K. Nomura

Fall 2019

Abstract

Regulation of listeriolysin O translation and c-di-AMP stress response in *Listeria monocytogenes*

by

Bret Nicholas Peterson

Doctor of Philosophy in Microbiology

University of California, Berkeley

Professor Daniel A. Portnoy, Chair

Listeria monocytogenes is a Gram-positive bacterial pathogen that cycles between life as a common environmental saprophyte and an intracellular pathogen of animals, including humans. It is a common model organism to study intracellular pathogenesis and mammalian immunity due to its amenability to genetic manipulation and undemanding growth requirements. Its diverse repertoire of lifestyles requires *L. monocytogenes* to be able to sense and respond to changing conditions quickly to maximize its fitness in all niches. Upon infection, bacteria must initiate a regulatory response during which its encoded virulence factors must be precisely coordinated in order to maximize survival. Listeriolysin O (LLO) is a pore-forming cytolysin and an essential determinant of virulence and its regulation through the pathogenic lifecycle is absolutely necessary. The synthesis of LLO protein is known to be regulated at the level of translation but the specific mechanism is unknown. This thesis will detail two individual projects that are linked by their common connection to translation.

LLO is responsible for freeing bacteria from host phagosomes and allowing them entry into the cytosol. In contrast to related toxins that are encoded by other bacterial pathogens, the regulation of LLO must be tightly regulated to allow for proper expression, which maximizes phagosome escape and prevents destruction of host plasma membrane integrity. For this reason, the regulation of LLO is believed to specifically promote the intracellular lifecycle of *L. monocytogenes*. Here we report that LLO synthesis is regulated by the formation of an extensive secondary structure of its mRNA (*hly*). This structure forms base-pair interactions between the ribosome binding site and a region in the coding region of the gene and affects translation. Genetic mutants that disrupt the secondary structure but maintain the amino acid sequence of the protein result in a virulence defect of as much as 10,000-fold in mice, and compensatory mutations almost completely restored virulence to WT levels. The nucleotide sequence of *hly* is selective to maintain maximum virulence while minimizing host cell death. We show that translational inhibition of LLO is growth phase dependent and that non-growing bacteria secrete proportionally more toxin than growing bacteria. Dependence on growth phase corresponds with a destabilization of the mRNA secondary structure in non-growing bacteria.

Cyclic di-AMP (c-di-AMP) is a nucleotide second messenger molecule in *L. monocytogenes* that is essential on rich media and coordinates the regulation of carbon flux through central

metabolism, osmotic turgor pressure and sensitivity to cell wall antibiotics. Its depletion is known to trigger the stringent response, which is characterized by the production of the alarmone (p)ppGpp and a re-structuring of protein synthesis at the translational and transcriptional level. Here we show that c-di-AMP binding protein B (CbpB), is an activator of the stringent response during low c-di-AMP conditions. Deletion of *cbpB* in the absence of c-di-AMP restores normal (p)ppGpp levels and its expression during low c-di-AMP levels raises alarmone levels. CbpB directly binds the stringent response-activating enzyme RelA and directs the accumulation of (p)ppGpp *in vitro*. These observations describe a novel non-canonical activation pathway of the stringent response and highlight the crosstalk between nucleotide signaling molecules in bacteria.

“Find what you love in life and let it kill you” – Charles Bukowski

Dedication

To my wife, Karly

Without whom I could not have achieved
anything in my adult life

Thank you for your love and support.

Table of contents

Chapter 1: Introduction to <i>Listeria monocytogenes</i>	1
Lifestyles of <i>Listeria monocytogenes</i>	2
<i>L. monocytogenes</i> determinants of virulence and LLO	2
The role of LLO in disease	3
LLO activity pH dependence	3
The LLO PEST-like sequence	4
Conclusion to LLO regulation	5
Introduction to codon usage	5
Introduction to the stringent response	6
Second messenger molecules and cyclic di-AMP	6
Chapter 2: Extensive N-terminal codon restriction of listeriolysin O is essential for <i>Listeria pathogenesis</i>	7
Introduction	8
Results	9
Identification of nucleotide complementarity between the hly PEST-encoding region and the 5'UTR	9
Genetic Analysis of the Predicted mRNA Structure.....	11
Effect of hly PEST and UTR mutants on <i>L. monocytogenes</i> pathogenesis	13
Complementation of S44S uncovers the trade-off between cytotoxicity and phagosomal escape	15
mRNA structure is regulated by growth phase	16
LLO synthesis and cell stress.....	19
Discussion	21
Supplementary Figures	22
Experimental Procedures	25
Chapter 3: CbpB activates the stringent response during low c-di-AMP conditions	33
Introduction	34
Results	35
Deletion of cbpB does not rescue cell wall defects in a Δ dacA background.....	35
CbpB is toxic to bacteria deficient in c-di-AMP	36
CbpB expression in the absence of cyclic di-AMP results in induction of the stringent response	37
Binding mode of c-di-AMP to CbpB.....	40
CbpB interacts with and activates the synthase region of RelA	42
Discussion	45
Experimental Procedures	47
Chapter 4: Concluding thoughts and future directions	52
LLO	53
c-di-AMP	55
Chapter 5: References	55

LIST OF FIGURES

Figure 1.1. The switch from saprophyte to intracellular pathogen.	2
Figure 2.1. PEST region codon restriction suggests an interaction between the ORF and the 5' UTR of the mRNA transcript	10
Figure 2.2. Genetic analysis of the predicted mRNA structure	12
Figure 2.3. Virulence of endogenous mutants in tissue culture and an animal model.....	14
Figure 2.4. Complementation of S44S through restoration of mRNA in a proximal site	16
Figure 2.5. Regulation of mRNA structure formation is growth phase dependent	18
Figure 2.6. Starvation does not affect <i>hly</i> translational de-repression	20
Figure S2.1. Virulence of PEST and UTR mutants.	22
Figure S2.2. Replicate DMSMaPseq structures	23
Figure 3.1. CbpB does not affect cell envelope defect in Δ acA mutants.	36
Figure 3.2. CbpB is toxic in the absence of c-di-AMP	37
Figure 3.3. CbpB induces the stringent response in the absence of c-di-AMP	39
Figure 3.4. Crystal structure of CbpB in complex with c-di-AMP	41
Figure 3.5. CbpB interacts with RelA and leads to increased (p)ppGpp	44

List of Tables

Table 2.1 <i>Lm</i> strains used in this study	27
Table 2.2 plasmids used in this study	28
Table 2.3 oligonucleotides used in this study	30
Table 3.1 SNPs identified from suppressor screen.....	38
Table 3.2 Positive interacting proteins identified through YTH	43
Table 3.3 Summary of data collection and refinement statistics	50
Table 3.4 <i>Lm</i> strains used in this study	51
Table 3.5 Plasmids used in this study	52

Acknowledgements

I would like to thank the Portnoy lab for their support throughout this process. Thomas, Aaron and Jon were both mentors and collaborators in my research and both were always excited to help. Aaron taught me how to appreciate bacterial genetics and that it was okay to geek out on esoteric science. Jon was a support beam who kept me going during hard times. Thank you all for accepting me into the lab and giving me the confidence to be a scientist. I'm honored that we could work together.

Brittney and Eric entered the lab with me, and we are finishing together. You were both great people to work with and fun guys to party with. I appreciate the times we had to grab a drink and talk. Chen and Sam were great mentors. They asked great questions and expressed genuine curiosity about my research. Your ideas helped make me a better thinker and your patience allowed me to grow. Alex is the great empathizer. Always a good listener. I'm glad we got to learn how to be dads at the same time. Ying helped me do some cool science that I would have never done on my own. Her careful work was super helpful and I'm glad you've found your way in the lab. Thank you to Dan for being supportive of my family and for allowing me to pursue my own goals. Your undergraduate class is the reason I joined your lab. The rest of the Portnoy lab was fun to be around and made the workplace something to look forward to. Thank you also to Neil for working hard and providing logistical support.

Special thanks to my undergraduate researcher of three years, Jeff. So smart and so nice. Thank you for all your help and for saving the c-di-AMP project. I'm sorry that I made you come to lab when you could have been doing great work for the community, like saving lives and helping the homeless. Your work ethic is inspiring for me. You're going to be a king.

To my collaborators and mentors: Megan, Wee, Yan, Josh, Shakun and Liang. They all had a role in helping me finish. I'm glad to have worked with you all.

Russell Vance and Dan Nomura were a terrific committee members who provided solid assistance, both scientifically and as mentors. Britt Glaunsinger is the reason I came to Berkeley for graduate school in the first place, and I owe her greatly. John Karijolic, my first mentor, imparted to me my first perspectives in science. Thank you all.

Bret Nicholas Peterson

Curriculum Vitae

Education

Ph.D. University of California, Berkeley

Microbiology, expected December 2019

Regulation of Listeriolysin O

Committee: Daniel A. Portnoy (Chair), Russell E. Vance, Daniel K. Nomura

B.Sc. University of California, Berkeley

Microbiology, 2014

3.73 GPA

Graduated with Honors in microbial biology and Distinction in the College of Natural Resources

Research Experience

University of California, Berkeley- Graduate Student Researcher, Portnoy lab, 05/2015-Present

- Researching an RNA-mediated regulatory mechanism of toxin expression in the enteric bacterial pathogen *Listeria monocytogenes*.
- Defining the molecular link between cyclic di-AMP and (p)ppGpp in *Listeria*.

Molecular Team Intern at Pendulum Therapeutics, 7/2019-9/2019

- Consulted on research strategies for a nascent scientific division and helped create infrastructure for the proposed experiments. Worked with a team to screen anaerobic bacteria through a pipeline for commercialization.

University of California, Berkeley- Undergraduate Researcher, Glaunsinger lab, 1/2013-6/2014

- Undergraduate researcher working on the role of KSHV ORF45 in transactivation of the HIV promoter.

Publications

- Nguyen BN, **Peterson BN**, Portnoy DA. Listeriolysin O: a phagosome-specific cytolysin revisited. *Cellular Microbiology* 2018
- Portman JL, Dubensky SB, **Peterson BN**, Whiteley AT, Portnoy DA. Activation of the *Listeria monocytogenes* Virulence Program by a Reducing Environment. *mBio* 2017
- Whiteley AT, Garelis NE, **Peterson BN**, Choi PH, Tong L, Woodward JJ, Portnoy DA. c-di-AMP modulates *Listeria monocytogenes* central metabolism to regulate growth, antibiotic resistance and osmoregulation. *Molecular Microbiology* 2017
- Karijolich J, Zhao Y, **Peterson B**, Zhou Q, Glaunsinger B. Kaposi's sarcoma-associated Herpesvirus ORF45 mediates transcriptional activation of the HIV-1 LTR via RSK2. *Journal of Virology* 2014

Manuscripts in preparation

- **Peterson BN**, Young M, Wang J, Whiteley AT, Woodward JJ, Luo S, Tong L, Wang JD, Portnoy DA. CbpB is a c-di-AMP dependent activator of the stringent response in Firmicutes. *In preparation*
- **Peterson BN**, Portman JL, Feng Y, Wang J, Portnoy DA. Extensive N-terminal codon restriction of listeriolysin O is essential for *Listeria* pathogenesis. *In preparation*

Selected Presentations

- **Peterson BN**, Portman JL, Feng Y, Portnoy DA. Interaction between the 5' UTR and Listeriolysin O ORF down-regulates expression to maximize virulence. ASM Microbe 2019, San Francisco, CA. *Poster*
- **Peterson BN**, Portnoy DA. *hly* mRNA structure fine-tunes listeriolysin O expression for *Listeria monocytogenes*. IDI Department Seminar 2019. *Oral presentation*
- **Peterson BN**, Portman JL, Feng Y, Portnoy DA. *hly* mRNA structure fine-tunes LLO expression. Bay Area Microbial Pathogenesis Symposium 2019. *Poster*
- **Peterson BN**, Portman JL, Feng Y, Portnoy DA. Interaction between the 5' UTR and *hly* ORF down-regulates expression. Gordon Research Conference: Microbial Toxins and Pathogenicity 2018. Waterville Valley, NH. *Poster*
- **Peterson BN**, Feng Y, Portnoy DA. The convergence of cyclic di-amp and (p)ppGpp. Bay Area Microbial Pathogenesis Symposium 2018. *Poster*
- **Peterson BN**, Glaunsinger B. Epigenetic regulation of the HIV-1 LTR by KSHV ORF45. Honors Research Presentation College of Natural Resources 2014. *Oral Presentation*

Teaching and Mentoring

- Graduate student instructor for Human Physiology and Bacterial Pathogenesis. Led multiple discussions sessions, designed lesson plans and quizzes, and moderated journal clubs for UC Berkeley undergraduates. – Spring 2016 & 2017
- Mentor to a highly skilled undergraduate researcher in the lab, who received the Summer Undergraduate Research Fellowship for his research. – 8/2016 - Present
- Mentored new Portnoy lab members including 3 graduate students and 2 postdocs. - 5/2015 - Present
- Tutor of the Bio 1A class at City College of San Francisco. Offering laboratory assistance and pre-exam study sessions. 1/2011 – 5/2011

Honors and Awards

- American Society of Microbiology Richard and Mary Finkelstein Travel Award, 3/2019
- National Science Foundation Graduate Research Fellow, 8/2015 - Present

- Undergraduate Fellowship: Sponsored Projects for Undergraduate Research (SPUR), 8/2013
- Qualified in submarines, 11/2005
- Honored Member of the Ancient Order of Shellbacks, 12/2005 - Eternity

Chapter 1: Introduction to *Listeria monocytogenes*

Portions of this chapter were published in

Brittney N Nguyen, Bret N Peterson, and Daniel A Portnoy. Listeriolysin O: A phagosome-specific cytolysin revisited. *Cellular Microbiology*, 2019

Lifestyles of *Listeria monocytogenes*

Listeria monocytogenes is a facultative bacterial pathogen that is a significant public health concern worldwide (1). Infections are usually caused by the consumption of contaminated food and can result in severe gastroenteritis, meningitis, stillbirth and miscarriage. Vulnerable populations include the elderly, the immunocompromised and the unborn. A major aspect of *L. monocytogenes* research is the switch between its pathogenic and saprophytic states. In its saprophytic state it lives on decaying organic matter the soil and plants, and it has evolved to grow in harsh environment such as cold temperature, high salt and varying pH (2). These adaptations make it a concern in the food processing industry and public health agencies. If consumed by animals, *L. monocytogenes* switches to its pathogenic state, which is characterized by its intracellular lifecycle (Fig. 1.1). This lifecycle along with its broad host range and genetic tractability have allowed for *L. monocytogenes* to become model to study intracellular bacterial pathogens (3).

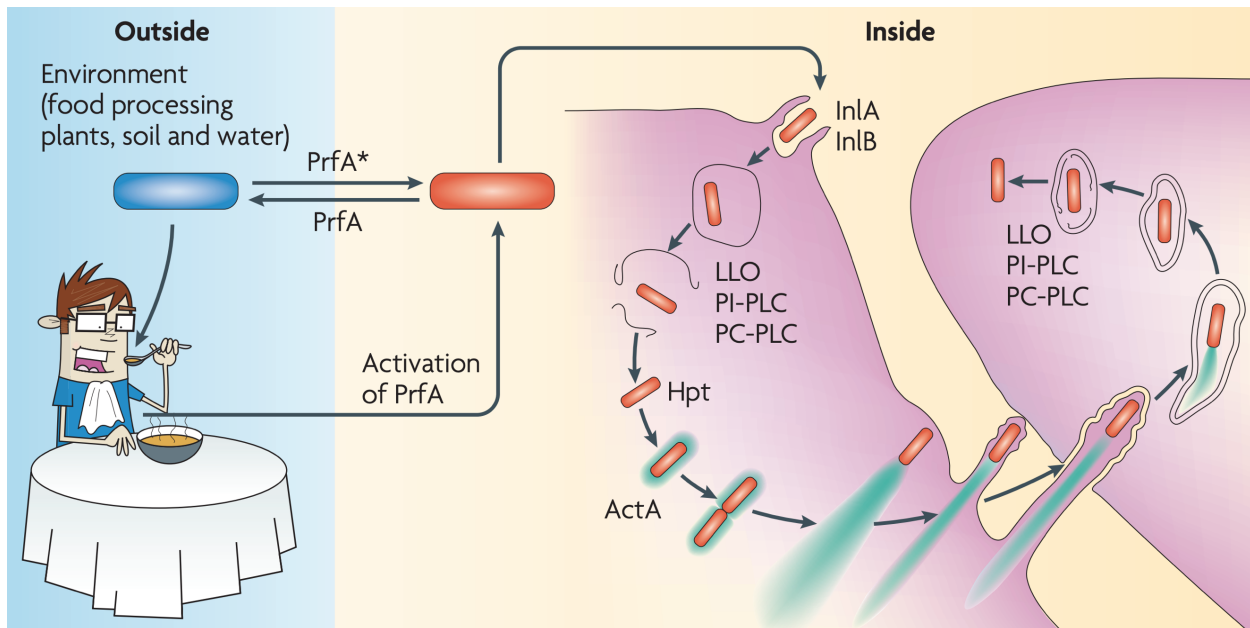


Figure 1.1. The switch from saprophyte to intracellular pathogen. From Freitag et al. (2)

L. monocytogenes determinants of virulence and LLO

The shift from saprophyte to pathogen must be carefully orchestrated to maximize virulence without sacrificing environmental fitness. Precise regulation of the virulence factors of *L. monocytogenes* is essential for bacterial survival. Bacterial pathogens typically encode a suite of virulence factors that promote their ability to replicate in their hosts while escaping host immunity (4). Though virulence factors between organisms can differ widely, many of them depend on similar strategies to cause disease (5). While some intracellular pathogens encode a multitude of effectors that are believed to function in maximizing virulence, *L. monocytogenes* is somewhat unique in that it requires relatively few to be pathogenic. The main virulence factors

sit on a 9-kb genomic island known as *Listeria* Pathogenicity Island 1 (LIPI-1) (6), which encodes six genes of known function.

The pathogenic lifecycle begins when *L. monocytogenes* is internalized by non-phagocytic cells or phagocytized by macrophages. Bacteria are initially trapped within a phagosome where they are unable to access the host cytoplasm or grow. They require the expression of the pore-forming cytolysin listeriolysin O (LLO, encoded by *hly*), with phospholipases (PlcA and PlcB) and metalloprotease (Mpl), to break free of the phagosome and reach the cytosol. Once free of the phagosome *L. monocytogenes* senses and responds to the host cytosol by activating the master virulence regulator (PrfA) (7). PrfA up-regulates expression of genes on LIPI-1 (8) including *actA*, leading to host actin-based motility and cell-to-cell spread (9).

Though each of these virulence factors has a specific function, none is more important for pathogenesis than LLO. Without LLO *L. monocytogenes* is 10,000-fold less virulent in mice and the bacteria are restricted to the extracellular environment of the host, where they are rapidly destroyed by the innate immune system (10). The following sections on LLO were published in Nguyen *et al.*

The role of LLO in disease

In humans, *L. monocytogenes* primarily causes self-resolving gastrointestinal infections. In immunocompromised individuals, *L. monocytogenes* can cause fatal systemic infections and, in pregnant women, placental infections that lead to pregnancy loss and systemic disease that results in death to the neonate (11). LLO is required for virulence in most if not all *L. monocytogenes* animal disease models, including acute systemic infection in mice, neonatal mice, pregnant mice, and pregnant guinea pigs (12-18). The requirement for LLO in virulence can be recapitulated in tissue culture where it is required for *L. monocytogenes* to escape from phagosomes. Mutants lacking LLO are unable to escape from the phagosome and consequently unable to grow intracellularly (9). In a mouse systemic infection model, LLO-negative mutants are 10,000-fold less virulent. The requirement for LLO in escape from the phagosome *in vivo* has been observed in real time in infected zebrafish (19). Strikingly, replacement of LLO with other CDCs results in strains that can escape from a phagosome but then kill the infected host cell, thereby eliminating the intracellular replicative niche (20-23). It is important to note that there are populations of *L. monocytogenes* that replicate extracellularly in the gut and gallbladder, and LLO is not required for the establishment of infection at these sites. However, although WT *L. monocytogenes* can disseminate from the gut to establish infection in systemic organs, LLO-deficient bacteria cannot efficiently disseminate from the gut to systemic sites (24-26).

LLO activity pH dependence

The optimal pH for LLO activity is 5.5, whereas extracellular CDCs such as PFO and SLO have similar activities at pH 5.5 and pH 7, suggesting that LLO has adapted to the specific setting of the acidified phagosome (22, 27). An early study into the molecular basis of this low optimal pH found that amino acid L461 was the main determinant and that this leucine is not conserved in CDCs from extracellular pathogens (28). Nonsynonymous mutations of L461 affect LLO activity and cytotoxicity. Mutants with a threonine substitution, the residue common in extracellular pathogen CDCs, were 100-fold less virulent in mice due to their increased

cytotoxicity. The pH insensitivity of L461T may be caused by an increase in the rate of oligomerization. Later, it was reported that LLO is denatured at neutral pH at temperatures greater than 30°C and that this was caused by charged amino acids within the transmembrane helices of Domain 3 that act as a pH sensor (29). Thus, although LLO is maximally active in acidified phagosomes, in the host cell cytosol, its activity is partially reduced, and it has the potential to denature. This mechanism is not solely responsible for limiting the activity of LLO to the phagosome, but it does contribute to reducing LLO-mediated cytotoxicity and preserving the replicative niche.

The LLO PEST-like sequence

The most distinctive and single largest contributing feature of LLO for the *L. monocytogenes*-specific lifestyle is a PEST-like sequence at the amino terminus of the protein (20, 30). PEST-like sequences were originally described in eukaryotic proteins with short half-lives and were thought to mediate those short half-lives, but it is now appreciated that they often include another domain known as a polyproline type II helix that mediates protein–protein interactions (31–33). Structural and *in vitro* analyses have indicated that residues in the polyproline type II helix region play a role in oligomerization through intermolecular contacts (31). Deletion of 26 amino acids of LLO that include the PEST-like sequence has a minor effect on hemolytic activity; however, the bacteria are extremely cytotoxic in tissue culture and 10,000-fold less virulent in mice (Decatur & Portnoy, 2000). Intracellular LLO exists in multiple forms, including 58 and 55 kDa molecular weight species. The lighter species is absent during infection with the PEST-deletion mutant or mutants deficient in actin-based motility, suggesting the PEST-like sequence contributes to subcellular compartmentalization or processing of LLO (34). Additionally, independently of the PEST-like sequence, LLO is ubiquitylated and accumulates as a ladder of higher molecular weight species in the presence of proteasome inhibitors. LLO has an N-terminal lysine that serves as a destabilizing signal for the N-end rule pathway, which involves ubiquitylation and proteasomal degradation. Indeed, the short intracellular half-life of LLO was extended by replacing the N-terminal lysine with stabilizing amino acids. However, the half-life extension only marginally affected cellular toxicity or virulence unless combined with mutations in the PEST-like sequence (35). Future studies should aim to identify the precise site or sites of ubiquitylation and their roles in pathogenesis and cell biology. Consistent with the hypothesis that the LLO PEST-like sequence is important for intermolecular interactions, the PEST-like sequence contains three residues (S44, S48, and T51) that are predicted targets for MAPKs, and one or all of these residues are important for LLO phosphorylation inside of infected host cells (34). Studies on phosphorylation of the PEST-like sequence have been confounded by the observation that point mutations in the region result in increased protein production and cytotoxicity and attenuated virulence (36). For example, mutations that change the S44 codon to alanine, thereby preventing phosphorylation, have increased translation of LLO. However, mutations that change the S44 codon to other serine codons also have increased translation, suggesting that the PEST-like sequence acts at the mRNA level to affect translation (see Chapter 2). Further evidence of translational regulation is supported by the observation that mutations in the 5'UTR alter protein expression (36, 37). The effect of mutations in the PEST-like sequence on translation complicates the study of post-translational modifications in the PEST-like sequence.

Conclusion to LLO regulation

Regulation of LLO is a complex process at the transcriptional, translational and post-translational level. While many advances have been made in understanding how LLO maximizes the virulence of *L. monocytogenes*, there are clearly unanswered questions that are hugely important for how intracellular pathogens generally establish their replicative niche. Chapter 2 addresses the question of LLO translation with implications for basic bacterial protein synthesis.

Introduction to codon usage

Gene expression in bacteria follows the basic tenets of most of life: DNA (the genetic material) is transcribed into RNA which is translated into proteins. This is referred to as the central dogma of molecular biology (38). In eukaryotes, transcription and translation are distinct processes that occur in separate compartments, whereas in bacteria these processes are tightly coupled such that translation can impact transcription (39). During transcription, mRNA is synthesized by RNA polymerase, which moves along the complementary DNA strand. This leaves free mRNA in its path to fold and eventually recruit the ribosome to begin translation. During translation, a ribosome binds a consensus sequence within the mRNA transcript called the ribosome binding site (RBS, aka Shine-Dalgarno sequence) and begins the energy intensive process of covalently linking amino acids to synthesize proteins.

The amino acid sequence of a protein is determined by triplets of nucleotides on the mRNA called codons. In all, there are 64 different possible combinations of codons (3 of which encode for stops), and all of them are utilized during protein synthesis. However, a basic question in all of life is why only 20 amino acids are used while there are 64 codons (40). This redundancy in coding capacity suggests that codon usage is not random and is of particular importance for gene expression. It has long been recognized that there are wide variations in the abundance of certain codons between organisms (41). Strikingly, the distribution of rare codons within individual genomes is not random, but cluster to distinct regions within ORFs (42).

A known phenomenon observed in all domains of life is N-terminal rare codon bias, wherein an organism's least common codons are over-represented at the 5' ends of ORFs. There are many hypotheses for N-terminal rare codon bias. Some stem from evidence that lower abundance codons slow translation rates (43). Slower translation rates might exert its influence on gene expression in multiple ways. First, slower translation in the 5' ends of genes is believed to slow early translation elongation in such a way that results in an overall increase in translational efficiency. This theory is known as the "codon ramp" hypothesis and is thought to optimize the spacing between ribosomes. Another hypothesis is that rare codons slow translation for targeting of secreted proteins to membrane insertion machinery to facilitate co-translational translocation. Evidence for this comes from the observation that secreted proteins are more highly enriched in 5' rare codons than cytosolic proteins (42). A third explanation for N-terminal rare codon bias is that mRNA itself regulates the translation rates through the formation of secondary structures that typically affect RBS accessibility. Several observational and experimental studies have indicated that it is mRNA folding that underlies N-terminal rare codon bias, and that rare codons per se are not the driving factors (44-46).

Introduction to the stringent response

The central dogma of molecular biology has distinct directionality, but exceptions to the rules exist. In one early experiment with *E. coli*, it was found that starving bacteria of amino acids resulted in a precipitous decrease in the amount of RNA (47), indicating that upstream processes in the central dogma could be affected by events downstream. This strain was said to have a “stringent response” to amino acid starvation. When a mutant was discovered that did not see a drop in RNA levels during starvation, it was termed a “relaxed mutant,” and contained a mutation in the relaxed (or *rel*) locus (48). It was later discovered that upon amino acid starvation the cell would synthesize new molecules called guanosine tetra- and pentaphosphate ((p)ppGpp) (49). Now it is appreciated that when bacteria are starved of amino acids, uncharged tRNAs enter the ribosome, and activate the synthesis of (p)ppGpp by the enzyme RelA, and the stringent response. This leads to a massive re-organization of resources away from synthesis of stable RNAs, ribosomes and protein production and towards the expression of biosynthetic genes. The stringent response is conserved throughout Bacteria, Archaea and even plants. It is also appreciated that the cause of the stringent response includes many other forms of starvation and cellular stress. (p)ppGpp is known as a nucleotide second messenger molecule and was one of the first to be discovered. Examples of its importance in maintaining homeostasis are legion.

Second messenger molecules and cyclic di-AMP

(p)ppGpp is a ubiquitous molecule in microbes but it is not the only nucleotide second messenger known. Other well-studied molecules include cAMP, with roles in carbon catabolite regulation, and cyclic di-GMP, with pleiotropic functions in cells. Recent work also discovered a family of eukaryotic-like synthases that are responsible for synthesizing a plethora of diverse molecules (50). Many of these molecules are believed to contribute to bacterial defense against phage (51). Cyclic di-AMP (c-di-AMP) is a molecule that was discovered for its ability to activate the mammalian innate immune response during infection with intracellular bacteria (52). c-di-AMP has roles in the regulation of the central metabolism cell turgor pressure and osmoregulation (53-55), and has been found to be essential on rich media (56), highlighting its importance to bacterial physiology and homeostasis. There are also links between c-di-AMP and (p)ppGpp that vary between bacteria (56-58).

While there are surely unelucidated functions of c-di-AMP in bacterial cells, it most often exerts its influence through inhibition of the target molecule (59). In *Listeria monocytogenes*, c-di-AMP binds and inhibits the activity of pyruvate carboxylase (PycA), the carnitine transporter OpuC (54, 60). The PII-like protein PstA binds c-di-AMP and has been proposed to act similarly to another PII protein, AmtB, which bind to the GlnK potassium channel and regulates its activity in an ATP, ADP, or 2-oxoglutarate-dependent manner (61-63). These examples in *L. monocytogenes* advance the trend in c-di-AMP-mediated regulation is that it acts as an inhibitor of other enzymes. The aim of this study is to understand the role of another c-di-AMP-binding protein CbpB.

Chapter 2: Extensive N-terminal codon restriction of listeriolysin O is essential for *Listeria pathogenesis*

Portions of this chapter are part of a manuscript in preparation:

Peterson BN, Portman JL, Feng Y, Wang J, Portnoy DA. Extensive N-terminal codon restriction of listeriolysin O is essential for *Listeria pathogenesis*. *In preparation*

Introduction

Intracellular pathogens are responsible for an enormous amount of world-wide morbidity and mortality (64). Though intracellular and extracellular pathogens can share virulence factors of similar mechanistic properties, strategies have evolved in each to establish and maintain their respective replicative niche (5). In many cases, pathogens must precisely regulate the expression of virulence factors dependent on time and space in order to maximize the virulence and prevent detection.

Listeria monocytogenes causes severe infections in humans and animals and is a model intracellular pathogen (65). An essential determinant of virulence for *L. monocytogenes* is the pore-forming cytolysin listeriolysin O (LLO), which is a member of an expansive group of bacterially encoded toxins called cholesterol-dependent cytolysins (CDCs) (66). After *L. monocytogenes* is phagocytosed, secreted LLO oligomerizes within the phagosomal membranes to form pores as large as 40 nm in diameter (67) and allows for the bacteria to reach the cytosol where they replicate and spread. LLO is essential for *L. monocytogenes* virulence, as mutants lacking the LLO gene (*hly*) are restricted to the phagosomal compartment and are therefore unable to replicate in the host. It is also unique compared to other CDCs in that it is the only one that is encoded by an intracellular pathogen and, thus, its expression and activity must be precisely regulated to facilitate the intracellular compartmentalization of *L. monocytogenes*. For example, the optimal pH for LLO activity is 5.5, whereas others are equally active at ranges between 5.5 and 7.0 (22, 27), indicating it has adapted to function most efficiently in the acidified vacuole. Substitution of LLO with another CDC results in bacteria that can escape the phagosome but causes cytotoxicity of the host cell due to loss of membrane integrity (20).

The most distinctive feature of LLO that separates it from other CDCs is the PEST-like domain encoded at its N-terminus (20). PEST-like domains were originally described in eukaryotic proteins and were thought to mediate shortened protein half-lives (32, 33). *L. monocytogenes* that encode *hly* lacking the PEST-like domain are 10,000-fold less virulent in mice due to overproduction of LLO and loss of host cell membrane integrity (20) (68), indicating an important role in the intracellular compartmentalization.

Although there has been extensive work to identify how the LLO PEST region affects LLO activity and turnover, it is also involved in toxin synthesis at the translational level. A synonymous mutation within the domain at S44 (TCT263AGC from the transcription start site) results in increased expression in broth due to elevated translational efficiency (68). The synonymous mutation results in a 10,000-fold decrease in virulence.

We have discovered that the mRNA transcript for LLO (*hly*) forms an extensive secondary structure between the PEST-encoding region and the 5' UTR. The codon for S44 base pairs directly with the ribosome binding site (RBS), resulting in a barrier to translation initiation. This secondary structure was confirmed with genetic non-coding mutations that either disrupt mRNA base pairing at the UTR or the PEST region or stabilize the structure in combination. We show that non-coding mutations can restore virulence of the PEST synonymous mutants to near WT levels, and that the nucleotide sequence of *hly* precisely maximizes vacuolar escape while minimizing host cytotoxicity. The mRNA structure changes between growing and non-growing states, such that the transcript becomes less structured at stationary phase with fewer base pair interactions proximal to the RBS. This corresponds with an increase in protein expression during stationary phase that occurs with *hly and* offers a mechanistic explanation for how codon usage regulates LLO compartmentalization.

Results

Identification of nucleotide complementarity between the hly PEST-encoding region and the 5'UTR

We wanted to understand how a single synonymous mutant in the coding region of *hly* could cause such a dramatic virulence defect. Analysis of the codon adaptation index (a measure of the deviation from codon usage in highly expressed genes) (69) showed that the PEST-encoding sequence indicated a lower score from *hly* as a whole (70) (CAI= 0.418 versus 0.534 respectively), but TCT263AGC actually reduced the score of the PEST region (CAI= 0.402), suggesting codon bias does not play a major role. To explore this codon specificity further we substituted the WT S44 codon with each of the other 5 serine codons and assessed the effect on protein secretion in broth. To maintain constant transcript levels, the endogenous promoter driving *hly* transcription was replaced with a constitutive promoter *Phyper(Pspac)* on an integrative plasmid (71) in a Δhly background. Five of the six serine codons resulted in LLO hyper-secretion from bacteria grown in broth (Fig 2.1B), indicating that the endogenous codon, UCU, is the only codon that supports WT expression. To test if this codon restriction was specific to the S44 codon, twenty-one non-coding mutations were made at different loci within the PEST-encoding region and many of these led to increased LLO secretion (Fig 2.1C).

We hypothesized that there might be an RNA regulatory element, perhaps a small RNA, that could affect translation of LLO. To investigate this possibility, we utilized RNApredator (72) to search for sites of complementarity to the PEST-encoding region of the transcript within the *L. monocytogenes* genome. Surprisingly, a low probability match was identified within the 5' UTR of the *hly* suggesting *cis* regulation. We used RNAfold (73) to model the structure of the *hly* transcript starting from the transcription start site to beyond the PEST-sequence. The generated structure showed base-pair interactions between the PEST-encoding sequence and the 5' UTR including the RBS (Fig 2.1A), suggesting a potential barrier to the efficient translation initiation of the gene that might result in reduced expression. mRNA folding stability at the 5' end has been shown to impact gene expression and underlie codon bias in bacteria, (45, 74). Folding stabilities of mRNAs is generally estimated by determining the folding free energies of the first *L* bases (ΔG_L). The predicted ΔG_{300} of this structure was -53.0 kcal/mol while that of the S44S (TCT263AGC) mRNA structure showed much lower probability interaction at the RBS with a folding free energy of $\Delta G_{300} = -49.5$ kcal/mol (Fig. 2.1D). These predictions suggest that *hly* is self-attenuated due to base pair interactions between the RBS and the PEST-encoding region of the ORF.

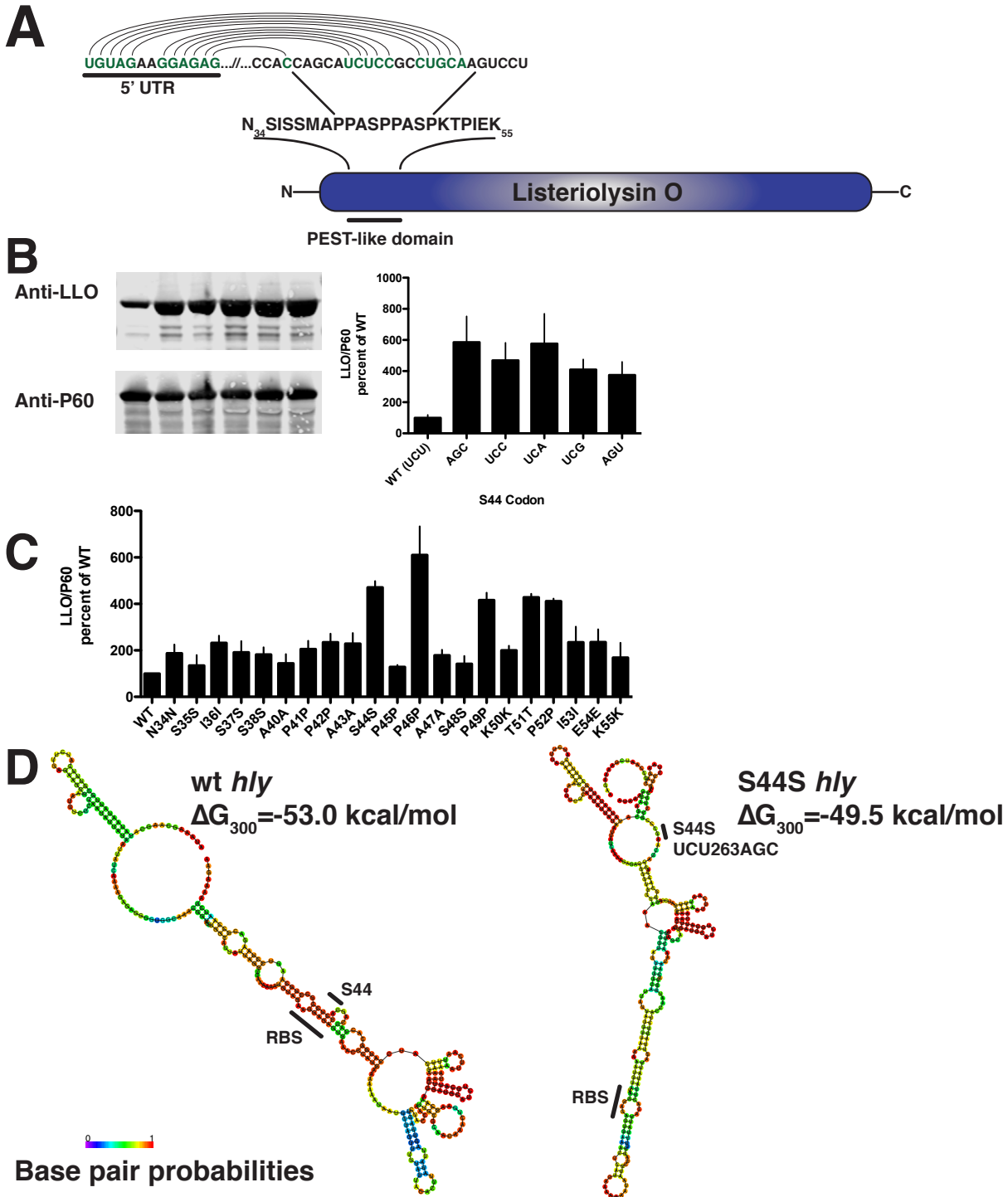


Figure 2.1. PEST region codon restriction suggests an interaction between the ORF and the 5' UTR of the mRNA transcript

(A) The LLO PEST-like domain and nucleotides with 5' complementarity (B) Representative western blot and quantification of LLO and P60 proteins from all synonymous S44S mutants. (C) Western blot quantification of LLO/P60 from additional PEST-encoding synonymous mutants in rich media. (D) RNAfold predicted mRNA structures and minimum free energies of WT *hly* and S44S (UCU263AGC). Red color indicates base pair probabilities.

Genetic Analysis of the Predicted mRNA Structure

To interrogate putative interactions between the UTR and the ORF, we performed a genetic mutational analysis of the *hly* mRNA. Our strategy was to introduce synonymous mutations within the PEST-encoding sequence and corresponding compensatory mutations in the 5' UTR that are predicted to restore the original base-pairing. Since the previously characterized S44S mutation is predicted to interact directly with the RBS, we chose to focus on downstream synonymous mutations that should base pair 5' to the RBS (Fig. 2.2A). P46 and A47 were selected and synonymous mutations were made to generate P46P and A47A (T271A and A274T respectively). Compensatory mutations were also constructed (UTR^{P46P} and UTR^{A47A}). Individual mutations in the 5' UTR or synonymous mutations in the PEST region led to an increase in protein secretion; however, when combined with their specific compensatory mutation, protein levels were restored to WT levels (Fig. 2.2B). Importantly, UTR compensatory mutations only complemented the ORF nucleotide to which they were predicted to interact. Transcript levels measured by RT-qPCR showed that RNA abundance did not significantly change between the mutants (Fig 2.2C), indicating that the basis of the difference in protein levels was most likely due exclusively to changes in translation efficiency and not RNA stability.

We also assessed LLO expression of an additional set of synonymous mutants, P46P* and A47A* (T271G and A274C respectively). These mutants change the GC content of *hly* and can presumably result in mRNAs with different folding free energies. The LLO expression profile of these strains behaved similarly (Fig. 2.2D). The mRNA abundance of the P46P* mutant was consistently elevated compared to WT (Fig. 2.2E). We hypothesized that this was a consequence of enhanced mRNA stability. To test this, we treated cells with rifampicin to inhibit RNA polymerase and measure the transcript stability. The P46P* transcript had 2x the half-life as WT (8.4 min and 4.5 min respectively), indicating that translation efficiency as well as RNA stability could be affected by these synonymous mutations (Fig. 2.2F).

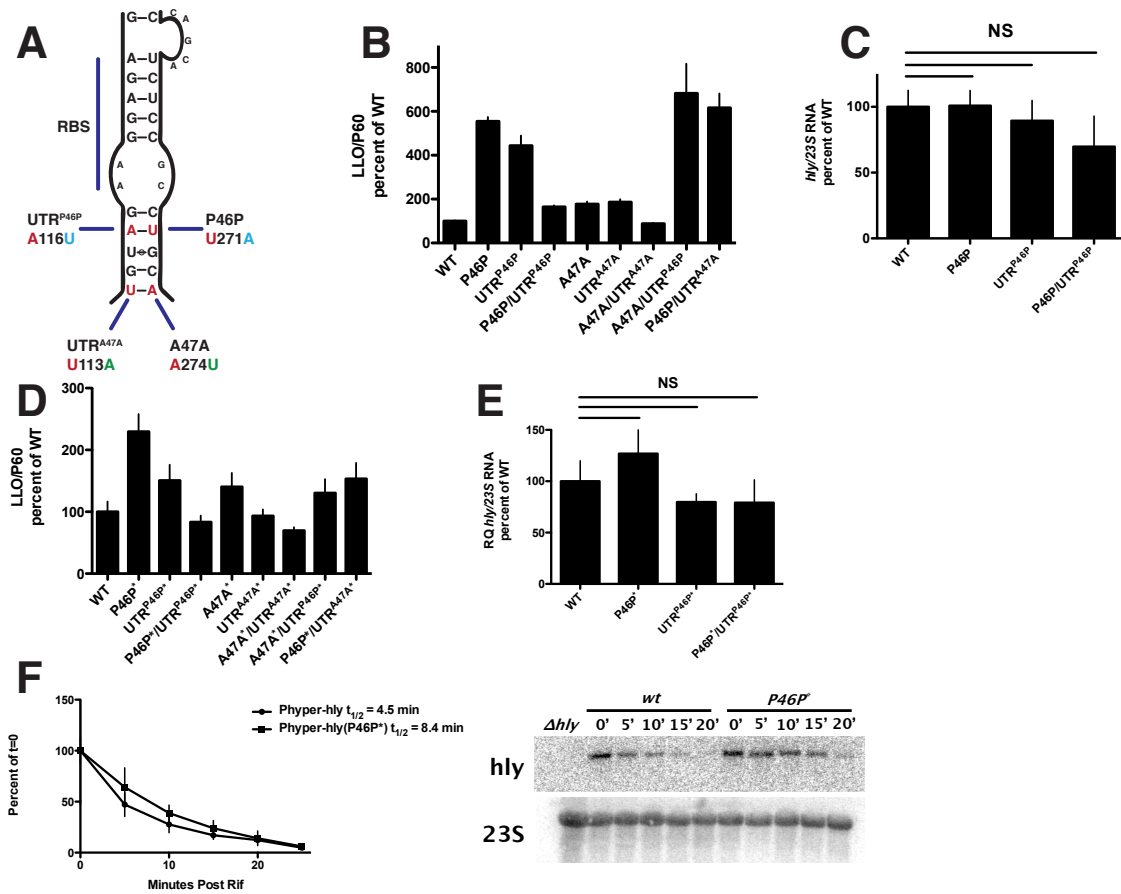


Figure 2.2. Genetic analysis of the predicted mRNA structure

(A) Close up diagram of the mRNA region to be analyzed. The mutated nucleotides were chosen based on proximity to the RBS and the codon capacity for mutations. (B) Western blot quantification of LLO/P60 from mutants expressing LLO from the Phyper promoter and grown in rich media. (C) mRNA transcript relative quantities (RQ) as a percent of WT. (D) Western blot quantification from mutants P46P* (U271G) and UTR^{P46P*} (A116C). (E) mRNA transcript relative quantities from GC mutants. (F) RT-qPCR and northern blot data showing the mRNA half-life for WT and P46P* transcripts. Error bars represent standard errors from 3 biological replicates. (NS= not significant by students t test ($P > .05$))

Effect of hly PEST and UTR mutants on L. monocytogenes pathogenesis

L. monocytogenes with synonymous mutations in the PEST region of LLO (e.g. S44S) escape from a phagosome but, due to mis-regulation of LLO synthesis, result in cytotoxicity of infected host cells (20). Here, we sought to characterize the consequences of infection with the corresponding UTR and double mutants by introducing the mutations into their chromosomal locus to assure native transcriptional regulation which is critical for *in vivo* virulence. First, we examined the interaction between the P46P synonymous mutant, its compensatory UTR mutation, and the double mutant during a cytotoxicity assay. In this assay, we infect marrow-derived macrophages (BMMs) and add gentamicin after 30 minutes to kill extracellular bacteria, then replaced with fresh media after 10 minutes to prevent killing of intracellular bacteria. After 6 hours cell supernatants are harvested to measure the lactate dehydrogenase activity. Consistently, each of the single mutants was extremely cytotoxic (Fig. 2.3A). We also measured bacterial growth in BMMs over 8 hours in media with gentamicin. Not surprisingly, both single mutants were dramatically decreased in CFU after 5h; which based on previous work, was due to the influx of gentamicin that occurs upon LLO-dependent cytotoxicity (Fig. 2.3E). In contrast, the double mutant grew like WT in BMMs and was less cytotoxic than either of the single mutants but was still more cytotoxic than WT (Fig. 2.3A,E). Strikingly, the double P46P*/UTR^{P46P*} (GC mutant) produced less cell death than WT, suggesting that the additional hydrogen bond in the CG interaction reduced expression of *hly* to less than WT (Fig. 2.3B). This also indicates that slight differences in LLO expression can result in large variations in cell death.

We further examined pathogenesis by monitoring the growth and cell to cell spread of the strains over 3d using a plaque assay in a monolayer of cells. In this assay, bacteria enter, grow and spread from cell-to-cell and after 3d, the monolayer is stained with neutral red, which stains only viable cells, and the plaque size is measured and compared to WT. Gentamicin is present during the 3-day assay to prevent extracellular growth of the bacteria. Based on previous work, strains that kill their host cell either fail to form a visible plaque or form smaller plaques. In this study, the PEST mutants were unable to form a visible plaque, while the corresponding UTR single mutant displayed much smaller plaques than WT (Fig. 2.3C). Unexpectedly, the A116C UTR mutant formed plaques similar in size to the double mutant, but they had decreased opacity, a phenotype we had not previously observed (Fig. 2.3D). The reduced opacity indicated a lower amount of cell death within the cells comprising the plaque, suggesting that *L. monocytogenes* is spreading, albeit at a reduced capacity, but fewer cells are killed, which we presume is due to the influx of gentamicin that kills the bacteria before they kill the host cell. The PEST/UTR double mutant was identical to WT in both plaque size and opacity, strongly suggesting that restoration of the WT mRNA structure and translational regulation during infection.

To assess the effect on *L. monocytogenes* virulence, we infected mice with the mutant bacteria by IV. The P46P synonymous mutant was 1000-fold less virulent in spleens and livers, while the UTR^{P46P} mutant was 100-fold reduced in both organs. Strikingly, the double P46P/UTR^{P46P} was as virulent as WT (Fig. 2.3F, S.2.1).

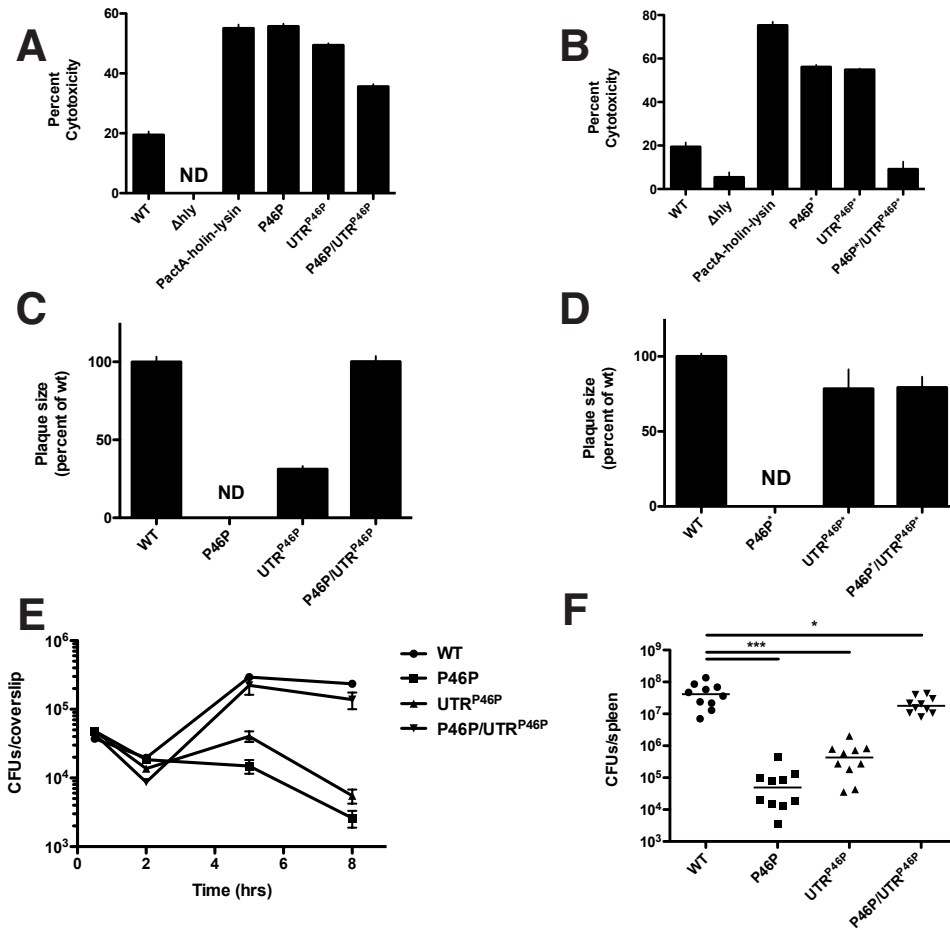


Figure 2.3. Virulence of endogenous mutants in tissue culture and an animal model

(A & B) LDH release assays in BMMs. Cells were washed 30 minutes post infection with media containing gentamicin for 10 minutes, washed 3x and incubated with gent-free media to prevent bacterial death. ND= not detected. (C) Plaque assay to measure cell to cell spread of AU mutants in L2 cells. (D) Plaque assay in GC mutants. UTR mutants formed plaques of decreased opacity, indicating less cytotoxicity despite cell-to-cell spread. (E) Growth curve in B6 BMDMs with gentamicin washed from the media. (F) Virulence of the mutant bacteria in CD-1 mice (iv dose= 10⁵) for 48 hrs. Significance was determined by unpaired t test. * = P ≤ 0.05, ** = P ≤ 0.01, *** = P ≤ 0.001.

Complementation of S44S uncovers the trade-off between cytotoxicity and phagosomal escape

Analysis of the previously characterized S44S mutant was complicated by its predicted interaction with the RBS. Therefore, to determine if WT function could be restored by making another silent mutation elsewhere in the gene, we chose to mutate nucleotides upstream of the predicted interacting site in the 5' UTR (AA111CT), that is predicted to extend, and therefore stabilize, the stem that is disrupted by S44S (Fig. 2.4A).

Quantification of the LLO produced from this strain indicated that this double nucleotide change was sufficient to reduce toxin production (Fig. 2.4B). To our astonishment, the AA111CT mutation restored the S44S strain from more than 10,000-fold less virulent in mice to near WT levels (Fig. 2.4C). Interestingly, the AA111CT mutant alone was attenuated in virulence by 10-fold, while LLO secretion from this mutant was less than WT. We hypothesized that by stabilizing the mRNA structure, LLO synthesis was reduced which might result in a phagosomal escape defect. Indeed, the AA111CT mutant had a phagosomal escape defect compared to WT, while the S44S mutant showed enhanced phagosomal escape (Fig. 2.4D). These results indicate that the *hly* nucleotide sequence controls the balance between cytotoxicity of host cells and phagosomal escape.

The decrease in LLO expression and corresponding drop in virulence caused by an *hly* AA111CT mutant was intriguing because we have not previously characterized such a strain. LLO-derived antigens are known class I MHC epitopes for cytotoxic T lymphocytes (CTL) (75) and we wondered how this mutant would affect adaptive immunity. *L. monocytogenes* induces a long lived CD-8⁺ -T-cell response that can be measured by challenging vaccinated mice with WT bacteria and measuring CFUs to assess protection (76). We mutated *hly* with the S44S, AA111CT and double mutant in a $\Delta actA$ background (the normal vaccination strain) and immunized mice with these strains. Interestingly, the $\Delta actA$ /AA111CT strain was able to protect against challenge better than $\Delta actA$ by CFUs in the liver, albeit not significantly different (Fig. 2.4E). The results of this experiment offer a potentially new vaccination strategy, wherein the immunization strain is attenuated for virulence and protects better than the normal immunization strain without the use of exogenous antigens.

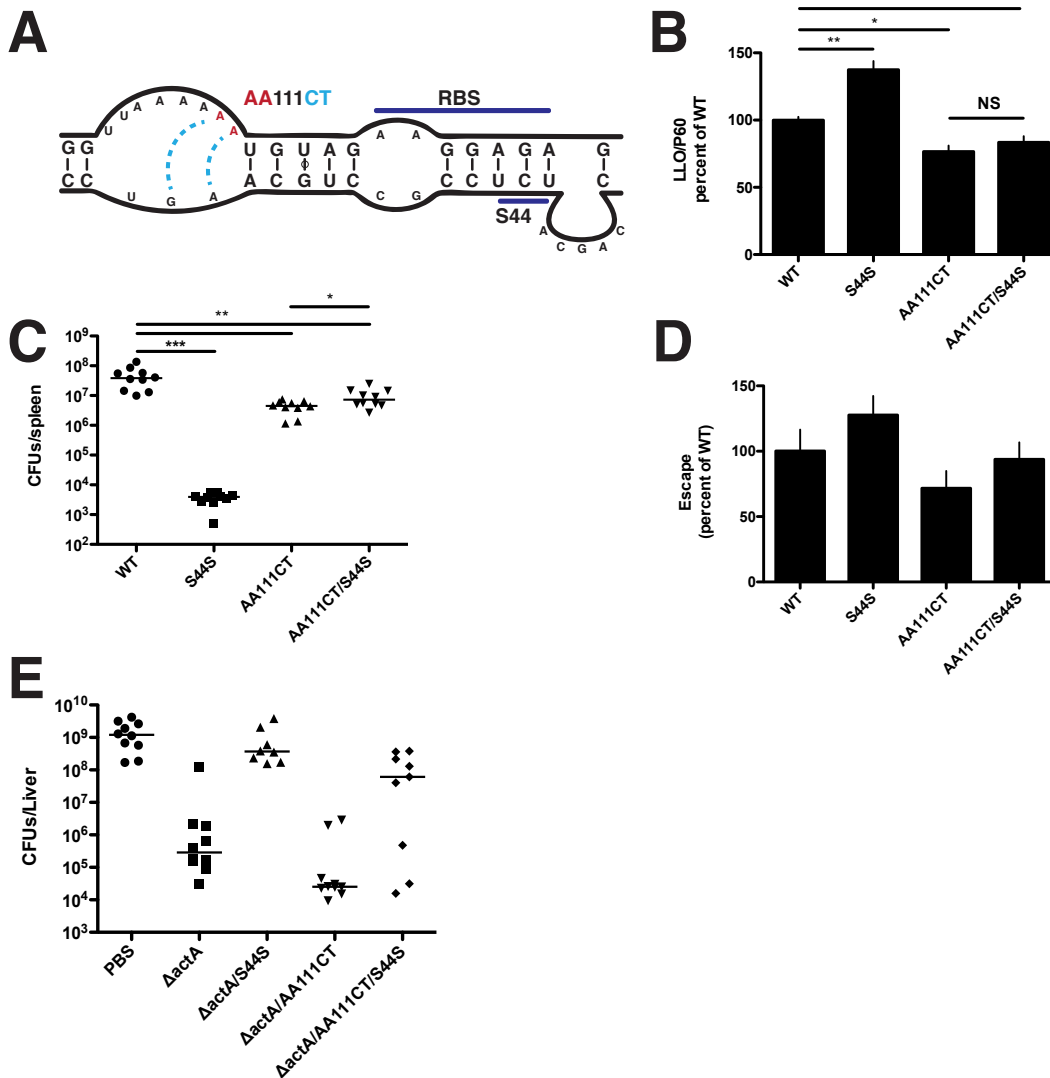


Figure 2.4. Complementation of S44S through restoration of mRNA in a proximal site

(A) The UTR of the endogenous locus was mutated at AA111CT from the TSS so that 5'-CU-3' would interact with 5'-AG-3', thereby stabilizing the disrupted *hly* structure. (B) Quantification of LLO secretion by western blot. (C) Infection of CD-1 mice (iv dose= 10⁵) for 48 hrs. (D) Phagosomal escape assay using co-localization of bacteria to P62 in the presence of cytochalasin D. (E) Challenge assay 30 days after vaccination with the indicated strains. Significance was determined by unpaired t test. * = P ≤ 0.05, ** = P ≤ 0.01, *** = P ≤ 0.001.

mRNA structure is regulated by growth phase

While it was an intriguing notion that codon bias could be the primary driver of *L. monocytogenes* virulence by the formation of a highly stable secondary mRNA structure, we suspected that there underlies a mechanism that controls a structural change in the mRNA. The mRNA transcript for *prfA* contains a thermosensor that alters its structure at 37°C, allowing for maximal translation efficiency at elevated temperatures (77). However, we found no change in LLO secretion profiles of our mutants at 25°C, 37°C, and 42°C (data not shown).

Since LLO is required for *L. monocytogenes* to escape from a phagosome, but is potentially lethal when expressed in the cytosol, it is reasonable to hypothesize that maximum LLO synthesis is required during starvation in a phagosome while translation is down-regulated during growth in the host cell cytosol to avoid cytotoxicity. Therefore, we examined the differences in LLO secretion from growing versus non-growing bacteria by pulsing with ³⁵S-methionine for 30 minutes and quantitating secreted LLO. While growing WT bacteria secreted much less LLO than the PEST mutant, non-growing bacteria produced equal amounts of LLO (Fig. 2.5A). These data indicated a reduction in LLO translation during bacteria growth.

To directly monitor changes in the mRNA structure during different growth states, we employed DMS-MaPseq to experimentally determine the *hly* structure during both conditions. DMS-MaPseq is a tool that uses the RNA-modifying properties of DMS and deep sequencing technology to determine the chemical accessibility of RNAs to modification. DMS methylates RNA nucleosides that are not engaged in a base pair interaction but is inaccessible to double stranded regions. The method relies on incorporation of mismatches at the methylation sites by the thermostable group II intron reverse transcriptase which can be identified by DNA sequencing. We found that during normal bacterial growth, a structure was formed that was nearly identical to the predicted structure. However, the DMS modification profile of the non-growing bacteria was much different and suggestive of a less structured RNA compared to that of growing bacteria (Fig. 2.5B). This lower stability structure corresponds with the higher relative protein production at stationary phase compared to bacteria that are growing.

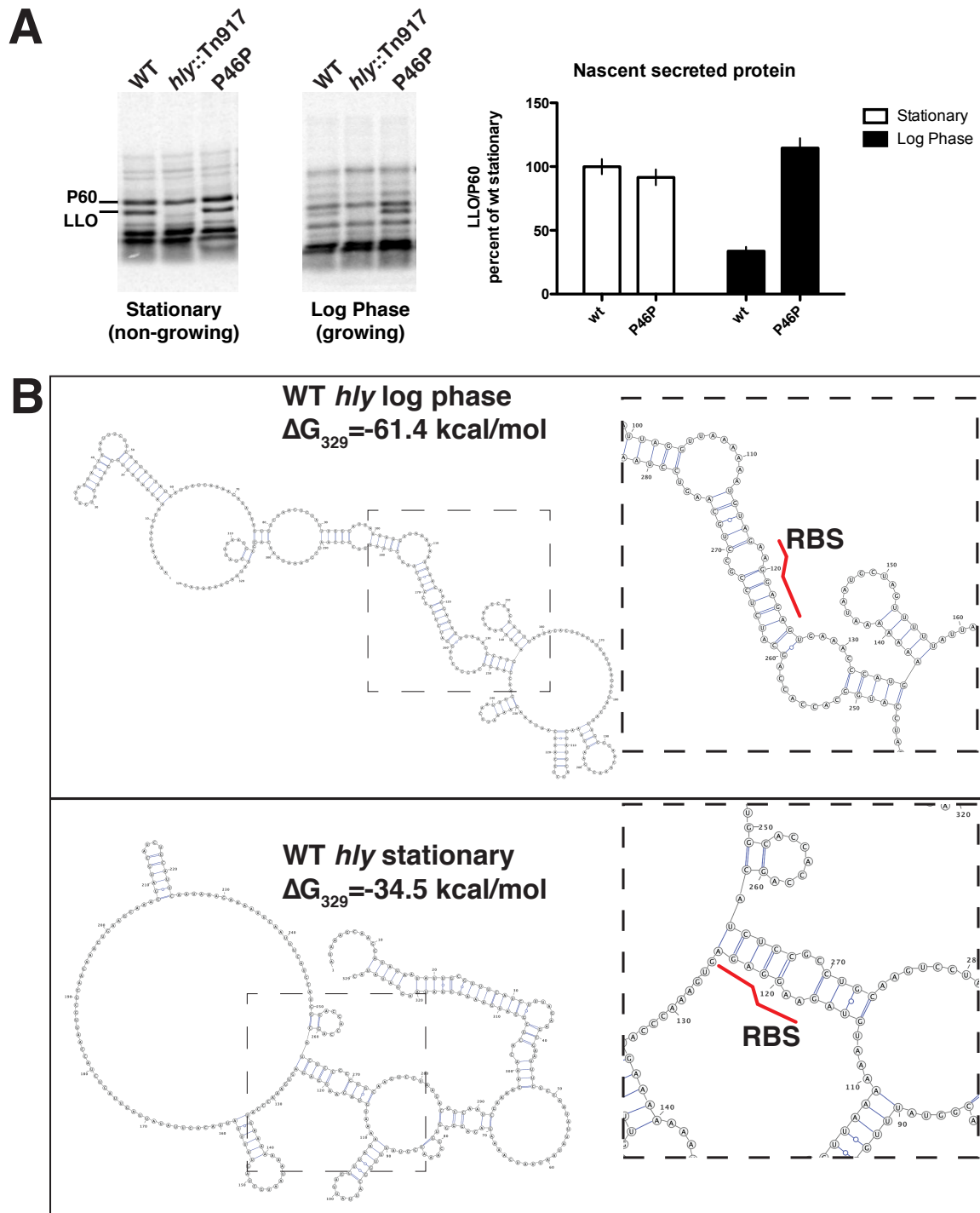


Figure 2.5. Regulation of mRNA structure formation is growth phase dependent

(A) Pulse labelling of EGDe *Listeria* with ^{35}S methionine in met^- synthetic media for 30 minutes in a growing or non-growing condition. Supernatants were TCA precipitated and analyzed for LLO/P60 levels. (B) Experimental

determination of *hly* mRNA structures by DMS-MaPseq of growing and non-growing bacteria. Minimum free energies of the first 329 nucleotides (ΔG_{329}) are shown next to the respective structures.

LLO synthesis and cell stress

The conditions of the phagosomal compartment and its effect on *L. monocytogenes* represent an unexplored area of research. We hypothesized that the reason that *L. monocytogenes* is unable to grow is that the bacteria are starving for nutrients. Pulsing bacteria with ^{35}S methionine for 30 minutes allows for dynamic analysis of secreted proteins. While we showed that non-growing bacteria in nutrient replenished media synthesize similar levels of protein regardless of the presence of synonymous mutations in the PEST region (Fig. 2.5A), performing the same experiment during true stationary phase with un-replenished media indicated the same result (Fig. 2.6A), though exactly quantifying the difference was technically different because LLO was the *only* protein secreted at high enough levels.

Serine hydroxamate (SHX) is an inhibitor of seryl-tRNA synthetase and is known to inhibit translation and induce the stringent response. Growing bacteria were incubated with SHX for 5 minutes prior to pulsing with methionine, to observe the effect of the stringent response on LLO synthesis. Although overall protein production was inhibited to some extent, the P46P PEST mutant produced more LLO than WT even when starved with SHX (Fig. 2.6B). This suggests that amino acid starvation does not relieve *hly* translational repression. Similar results were obtained during incubation with methyl α -D-glucopyranoside (α MG), which induces the stringent response through carbon starvation (Fig. 2.6C). Together, these data indicate that *hly* translational de-repression is not mediated simply inducing stresses in growing bacteria and suggest that other factors during stationary phase play a role.

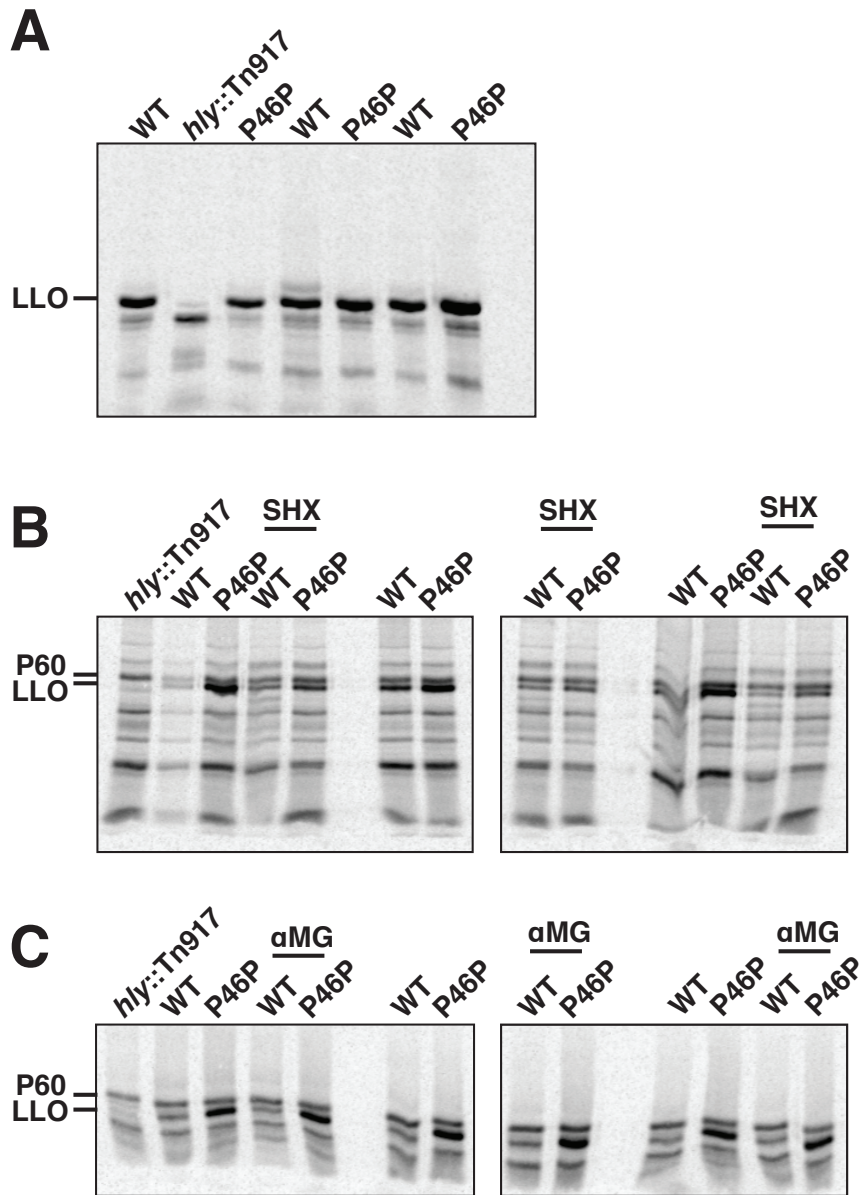


Figure 2.6. Starvation does not affect *hly* translational de-repression

(A) 30-minute pulse of ^{35}S methionine during true stationary phase in spent media. LLO secretion is the same for WT and PEST mutant. (B) Incubation with SHX during methionine pulse. (C) Incubation with α MG during methionine pulse.

Discussion

The results of this study indicate that *hly* regulation occurs at the translational level by forming an RBS-occluding secondary structure between the 5' UTR of the mRNA and the ORF. While disruption of this structure by introduction of non-coding mutations has little effect on transcript levels, the changes in toxin synthesis can be large enough to result in avirulent bacteria, indicating that the formation of this structure is one of the most important mechanisms of virulence regulation for this pathogen. We showed that toxin expression is precisely controlled at the nucleotide level to balance between maximizing phagosomal escape without killing host cells. The structure of *hly* was confirmed by biochemical probing, which showed that it changes between growing and non-growing conditions, providing a window into the regulation occurring between intracellular compartments.

mRNA secondary structure at regions proximal to the RBS has been well-documented to influence protein synthesis by interfering with translation initiation (78). Recently, observational and high-throughput experimental studies demonstrated that low mRNA folding stability at the 5' ends underlies the phenomenon of rare codon bias that exists in all domains of life (44). The results of this study suggest that control of *hly* translation is governed by the codon usage in the PEST region, which is selective to maintain a mRNA structure that maximizes virulence and cell-to-cell spread. Though codon biases are highlighted in association with promoting translation, here, codons are restricted to form a highly stable mRNA molecule to reduce LLO synthesis.

We observed LLO synthesis to be growth phase dependent, such that non-growing bacteria, like those restricted to the phagosome, produce more toxin than growing bacteria due to an mRNA structural change that increases accessibility to the RBS. While growth *rate* has been shown to affect the ability of the *E. coli ompA* 5' UTR to regulate its own mRNA stability (79, 80), in this case the secondary structure exerted its influence by protection from RNase-mediated degradation, not RBS occlusion.

The differences in a bacterial cell structure between stationary phase and exponentially growing bacteria are numerous and an area of exciting research. Upon starvation, the stringent response is induced and the total number of active ribosomes in the cell decreases (81), concomitant with a reduction in protein synthesis (82). However, the vast majority of non-growing bacteria in a starving population are able to produce protein at a constant rate up to 60 hours after entry into stationary phase (83).

Single molecule fluorescence microscopy studies show that the transcription, translation and membrane insertion (called transertion) machinery becomes stratified in fast growing cells(84); with RNA polymerase localizing to foci in the nucleoid and ribosomes rich area at the periphery of cells. In *Bacillus subtilis*, ribosomes in fast growing cells occupy the poles and mid-cell future division sites, while ribosomes at stationary phase are more diffuse(85).

Co-transcriptional translation (coupling) is a major piece of the transertion chain that has been shown to regulate 5' end mRNA-mediated RBS occlusion in *E. coli folA* (45). And in classical experiments, the importance of coupling is evident in the regulation of the histidine operon (86) (39). Understanding the extent of transertion chain disruption during no-growth conditions may hold answers important for *L. monocytogenes* pathogenesis.

Supplementary Figures

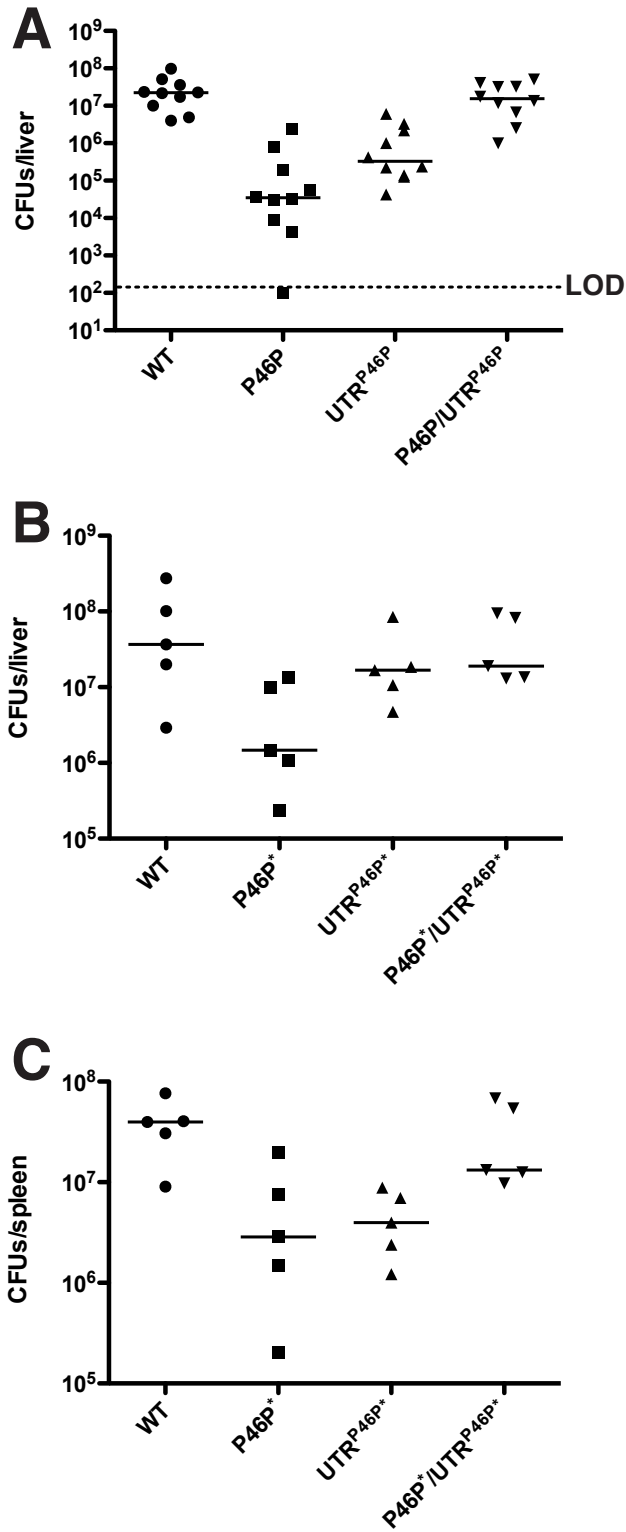


Figure S2.1. Virulence of PEST and UTR mutants.

(A,B,C) Virulence of the indicated strains of bacteria in CD-1 mice (iv dose= 10⁵) for 48 hrs.

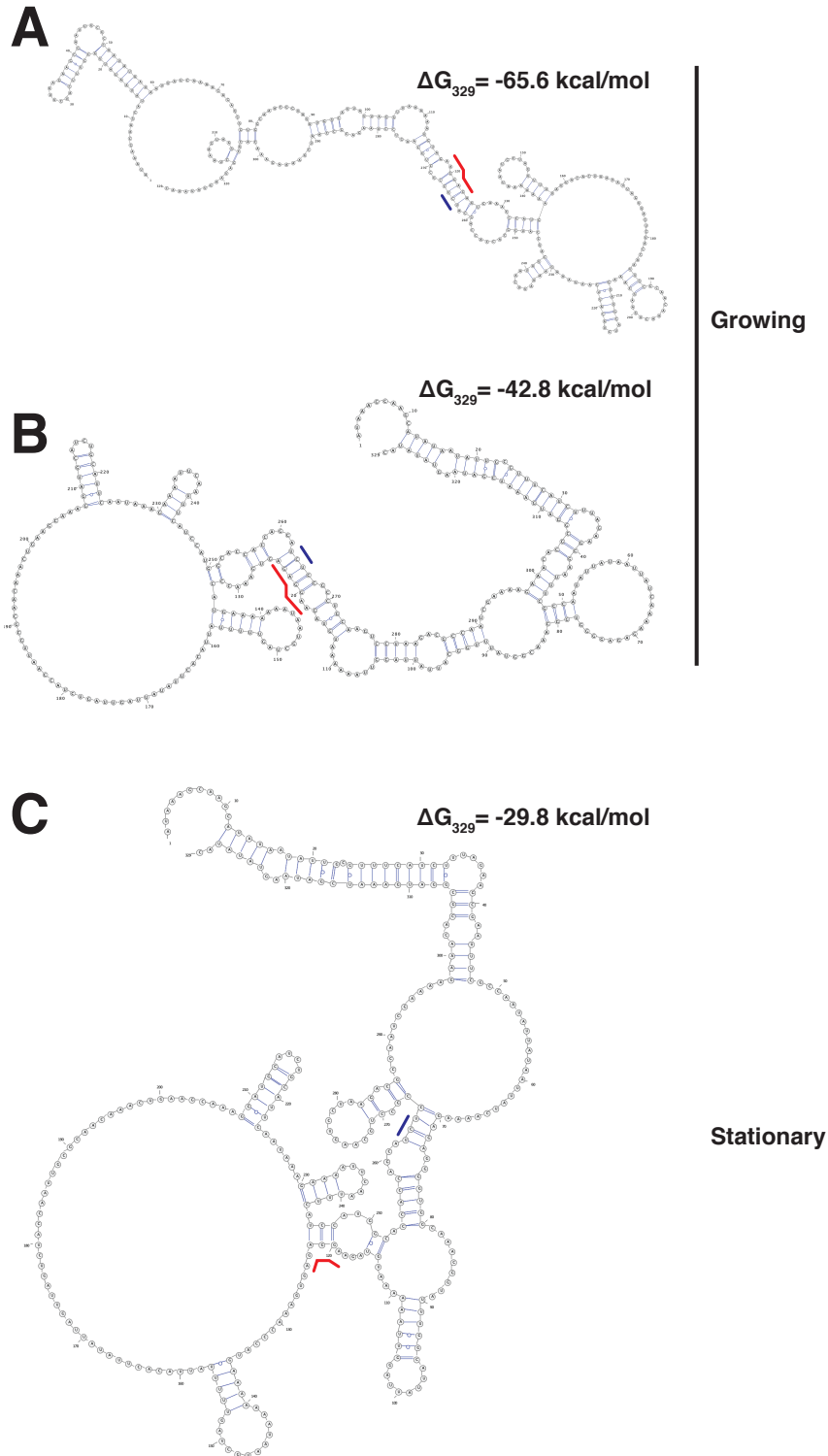


Figure S2.2. Replicate DMSMaPseq structures

A & B) WT *hly* structures from growing *L. monocytogenes*. The RBS forms a base pair interaction with the PEST-encoding region that extends in the 5' and 3' direction from the translation initiation site C) Additional structure

from stationary bacteria. The region immediately downstream of the RBS is not predicted to form a base pair interaction, resulting in reduced stability. Red line segments indicate the RBS, Blue line segments indicate the S44 codon. Nucleotides 1-329.

Experimental Procedures

Bacterial strains and growth conditions

Listeria monocytogenes (WT 10403S and its derivatives)(**Table 1**) were grown in Brain Heart Infusion (BHI; BD Biosciences) at 37°C. EGDe strains were grown in methionine⁻ *Listeria* Synthetic Media (LSM). Growth occurred aerobically at an RPM of 220. Growth was measured by optical density at a wavelength of 600nm (OD₆₀₀). Frozen bacterial stocks were stored in BHI + 40% glycerol at -80°C. Antibiotics were used at the following concentrations 200 µg/ml and chloramphenicol at 7.5 µg/ml for *L. monocytogenes* and 10 µg/ml for *E. coli*. Derivative strains were made using primers on Table 2.3 using pPL2 for knock-ins and pKSV7 for allelic exchange.

In vitro LLO quantification

Overnight cultures were washed and back diluted into fresh media at 1:20 and allowed to grow for 6 hours at 37°C shaking. Cultures were pelleted and supernatants were treated with trichloroacetic acid (TCA) at 10% for 1 hour on ice to precipitate protein. Supernatants were centrifuged at 13K rpm for 15 minutes and pellets were washed with acetone, followed by a 12-minute centrifuge. These pellets were washed a final time in acetone and washed for 10 minutes. Pellets were allowed to dry overnight or in a vacuum and resuspended in 1X lithium dodecyl sulfate (LDS) buffer (Invitrogen) containing 5% β-mercaptoethanol (BME). Secreted protein was boiled for 5 minutes and separated on by SDS-PAGE. The primary antibodies, a rabbit polyclonal antibody against LLO and a mouse monoclonal antibody against P60 (Adipogen), were each used at a dilution of 1:5,000. P60 is a constitutively expressed bacterial protein used as a loading control for secreted proteins. Secondary antibodies were goat anti-mouse IRDye 800CW (Licor) and Alexa Fluor 680 goat anti-rabbit (Life Technologies). All immunoblots were visualized using the Odyssey imager and quantified using ImageJ. For labelling experiments, EGDe strains were grown in Met⁻ LSM until stationary and either diluted in fresh Met⁻ LSM, grown for 6 hours (5-hour doubling time) and pulsed with EasyTag ³⁵S-Methionine (Perkin Elmer) at 25µCi/0.1 O.D.₆₀₀, or pulsed at stationary. The pulse lasted for 30 minutes followed by TCA precipitation of supernatants as described above.

RT-qPCR

Bacteria were grown to mid-log (OD₆₀₀ of 0.8) and RNA was isolated by RiboPureTM-Bacteria RNA isolation kit (ambion). RNA was DNase treated, followed by phenol chloroform extraction and cDNA synthesis using iScript reverse transcriptase (Bio-Rad). qPCR was performed with Kapa SYBR fast (Kapa Biosystems) using the manufacturer's recommended cycle using primers from Table 2.3.

Tissue culture experiments using BMMs

Bacteria were grown at 30°C shaking overnight. Overnight cultures were washed and re-suspended at 1/10 in PBS. This was used to infect a monolayer of murine bone marrow derived macrophages at a MOI of 0.25 that had been seeded the previous day on glass coverslips. Cells were washed three times 30 minutes post infection and media was replaced. At 1 hour, gentamicin was added to the tissue culture media to kill the extracellular bacteria (50µg/ml). Coverslips were collected in water and plated to innumerate CFUs. For cytotoxicity assays, monolayers of PAM3CSK-treated BMMs were infected with bacterial strains for 30 minutes,

washed three times in DPBS, followed by incubation with gentamicin-containing media (50 µg/ml) for 10 minutes. Cells were washed again 3X and fresh media was replaced without gentamicin. At 6 hpi supernatants were isolated and analyzed as previously described (87). Results are presented as a percentage of 100% cell death as determined by cells treated with 1% Triton X.

Phagosome escape assay

Murine bone marrow-derived macrophages (BMMs) were seeded on glass coverslip within 24-well plate at 2×10^5 cells per well and allowed to adhere overnight in TC chamber. Bacteria were grown in BHI at 37 °C overnight with shaking and subcultured 1:20 until reaching an OD₆₀₀ of 1.0. To target cytosolic bacteria efficiently, 250 ng/ml cytochalasin D (cytD, Sigma) was added to BMMs 30 min before infection to prevent actin polymerization and was maintained in media throughout infection. BMMs were infected at a MOI of 10 for 30 min, washed twice prior to replacing fresh BMM media with cytD, and 50 µg/ml gentamicin was added to kill the extracellular bacteria at 1 h post-infection. Coverslips were removed and proceeded to immunostaining as previously described (Gabe, PNAS 2017) at 1.5 h post-infection. Primary antibodies recognizing *L. monocytogenes* (1:1000 dilution; BD Biosciences, no. 223021) and BMM protein p62 (1:200 dilutions; Fitzgerald, no. 20R-PP001) were used and detected with fluorophore conjugated secondary antibodies, rhodamine red-X goat anti-rabbit IgG (1:2000 dilution; Invitrogen, R6394) and AlexaFluor-647 goat anti-guinea pig IgG (1:2000 dilution; Invitrogen, A21450). Coverslips were mounted in Prolong Gold antifade reagent with DAPI (Invitrogen, P36935), and imaged with BZ-X710 KEYENCE microscope. Bacteria co-localized with p62 were counted as cytosolic ones that successfully escaped from phagosomes. More than 100 bacteria per sample were analyzed.

Mouse infections

8-week-old CD-1 outbred mice (Charles River) were infected intravenously with 1×10^5 CFUs in 200 µl of PBS. Animals were sacrificed at 48 hours and spleens and livers were harvested in 5 ml or 10 ml in 0.1% IGEPAL CA-630 (Sigma) in water, respectively, and plated for enumeration of bacterial burdens.

hly structure probing using DMS-MaPseq

Bacteria were grown in BHI from OD~0.01 to OD~0.5 and treated with DMS (15 ml culture to 700 µl DMS) for 2 minutes at 37 °C shaking. Non-growing bacteria were grown to stationary (12-18 hours) The DMS was then deactivated with a solution of 30% BME (Sigma), 25% Isoamyl alcohol, washed with 30% BME and then centrifuged to pellet the bacteria which was flash frozen. DMS-treated RNA was extracted with Zymo Research Quick-RNA Fungal/Bacterial kit and reverse transcribed with an *hly*-specific primer (Table 3), First Strand buffer (Invitrogen), 1mM dNTP, 10mM DTT, 10U SUPERase In (Ambion), and 100U TGIRT-III enzyme (InGex) for 1.5 hours at 57 °C, followed by 85 °C for 5 min. RNA was removed by adding 5U RnaseH and incubating for 20 mins at 37 °C. cDNA was amplified by PCR using primers (Table 3). These amplicons were <500 bps in length. These were deep sequenced at the Vincent J Coates Genomics Sequencing Laboratory using an Illumina MiSeq 300PE V3 platform. Analysis of the sequencing data was conducted using Detection of RNA folding Ensembles using Expectation-Maximization clustering (DREEM) (Rouskin lab). This consisted of mapping reads to *hly* on the 10403S reference genome, creating bit vectors from aligned

reads, and clustering the bit vectors using an Expectation-Maximization algorithm. The analyzed region of the transcript is from nucleotides 39-306. The output structures are displayed in figures 4 and supplementary figure 6.

Table 2.1 *Lm* strains used in this study

Strain Number	Genotype	Source
DP-L184	WT 10403S	(88)
DP-L2161	<i>Δhly</i>	(21)
DP-L4515	S44S (<i>TCT263AGC</i>)	(68)
DH-L911	<i>Δhly pPL2-Phyper-hly</i>	(37)
DP-L6808	<i>Δhly pPL2-Phyper-hly(TCT263AGC)</i> S44S	This study
DP-L6809	<i>Δhly pPL2-Phyper-hly(TCT263TCC)</i> S44S	Schnupf
DP-L6810	<i>Δhly pPL2-Phyper-hly(TCT263TCA)</i> S44S	This study
DP-L6811	<i>Δhly pPL2-Phyper-hly(TCT263TCG)</i> S44S	This study
DP-L6812	<i>Δhly pPL2-Phyper-hly(TCT263AGT)</i> S44S	This study
DP-L6813	<i>Δhly pPL2-Phyper-hly(AAT233AAC)</i> N34N	This study
DP-L6814	<i>Δhly pPL2-Phyper-hly(TCA236TCG)</i> S35S	This study
DP-L6815	<i>Δhly pPL2-Phyper-hly(ATT239ATC)</i> I36I	This study
DP-L6816	<i>Δhly pPL2-Phyper-hly(TCA242TCG)</i> S37S	This study
DP-L6817	<i>Δhly pPL2-Phyper-hly(TCC245ACG)</i> S38S	This study
DP-L6818	<i>Δhly pPL2-Phyper-hly(GCA251GCG)</i> A40A	This study
DP-L6819	<i>Δhly pPL2-Phyper-hly(CCA254CCG)</i> P41P	This study
DP-L6820	<i>Δhly pPL2-Phyper-hly(CCA257CCG)</i> P42P	This study
DP-L6821	<i>Δhly pPL2-Phyper-hly(GCA260GCG)</i> A43A	This study
DP-L6822	<i>Δhly pPL2-Phyper-hly(GCG266CCC)</i> P45P	This study
DP-L6823	<i>Δhly pPL2-Phyper-hly(CCT269CCG)</i> P46P*	This study
DP-L6824	<i>Δhly pPL2-Phyper-hly(CCT269CCA)</i> P46P	This study
DP-L6825	<i>Δhly pPL2-Phyper-hly(GCA272CCC)</i> A47A*	This study
DP-L6826	<i>Δhly pPL2-Phyper-hly(GCA272CCT)</i> A47A	This study
DP-L6827	<i>Δhly pPL2-Phyper-hly(AGT275TCG)</i> S48S	This study
DP-L6828	<i>Δhly pPL2-Phyper-hly(CCT278CCG)</i> P49P	This study
DP-L6829	<i>Δhly pPL2-Phyper-hly(AAG281AAA)</i> K50K	This study
DP-L6830	<i>Δhly pPL2-Phyper-hly(ACG284ACC)</i> T51T	This study
DP-L6831	<i>Δhly pPL2-Phyper-hly(CCA287CCC)</i> P52P	This study
DP-L6832	<i>Δhly pPL2-Phyper-hly(ATC290ATT)</i> I53I	This study
DP-L6833	<i>Δhly pPL2-Phyper-hly(GAA293GAG)</i> E54E	This study
DP-L6834	<i>Δhly pPL2-Phyper-hly(AAG296AAA)</i> K55K	This study
DP-L6835	<i>Δhly pPL2-Phyper-hly(A116U)</i> UTR ^{P46P}	This study
DP-L6836	<i>Δhly pPL2-Phyper-hly(A116C)</i> UTR ^{P46P*}	This study
DP-L6837	<i>Δhly pPL2-Phyper-hly(A116U)</i> UTR ^{P46P}	This study
DP-L6838	<i>Δhly pPL2-Phyper-hly(A116U/U271A)</i> P46P/UTR ^{P46P}	This study
DP-L6839	<i>Δhly pPL2-Phyper-hly(A116C/U271G)</i> P46P*/UTR ^{P46P*}	This study
DP-L6840	<i>Δhly pPL2-Phyper-hly(U113A)</i> UTR ^{A47A}	This study
DP-L6841	<i>Δhly pPL2-Phyper-hly(U113G)</i> UTR ^{A47A*}	This study
DP-L6842	<i>Δhly pPL2-Phyper-hly(U113A/A274U)</i> A47A/UTR ^{A47A}	This study
DP-L6843	<i>Δhly pPL2-Phyper-hly(U113G/A274C)</i> A47A*/UTR ^{A47A*}	This study
DP-L6844	<i>Δhly pPL2-Phyper-hly(A116U/A274U)</i> A47A/UTR ^{P46P}	This study
DP-L6845	<i>Δhly pPL2-Phyper-hly(A116C/A274C)</i> A47A*/UTR ^{P46P*}	This study
DP-L6846	<i>Δhly pPL2-Phyper-hly(U113A/U271A)</i> P46P/UTR ^{A47A}	This study

DP-L6847	<i>Δhly pPL2-Phyper-hly(U113G/U271G) P46P*/UTR^{A47A*}</i>	This study
DP-L6848	<i>hly(CCT269CCA) P46P</i>	This study
DP-L6849	<i>hly(CCT269CCG) P46P*</i>	This study
DP-L6850	<i>hly(A116U) UTR^{P46P}</i>	This study
DP-L6851	<i>hly(A116C) UTR^{P46P*}</i>	This study
DP-L6852	<i>hly(A116U/U271A) P46P/UTR^{P46P}</i>	This study
DP-L6853	<i>hly(A116C/U271G) P46P*/UTR^{P46P*}</i>	This study
DP-L6854	<i>pPL2-PactA-holin/lysin</i>	(87)
DP-L6855	<i>hly(AA111CT)</i>	This study
DP-L6856	<i>hly(AA111CT/ TCT263AGC) AA111CT/S44S</i>	This study
DP-L3633	EGDe	
DP-L6857	EGDe <i>hly::Tn917</i>	This study
DP-L6858	EGDe <i>hly (CCT269CCA) P46P</i>	This study
DP-L6859	<i>ΔRNaseIIIΔhly pPL2-Phyper-hly</i>	This study
DP-L6860	<i>ΔRNaseIIIΔhly pPL2-Phyper-hly(CCT269CCG) P46P*</i>	This study
DP-L6861	<i>ΔRNaseIIIΔhly pPL2-Phyper- hly(A116C) UTR^{P46P*}</i>	This study
DP-L6862	<i>ΔRNaseIIIΔhly pPL2-Phyper- hly(A116C/U271G) P46P*/UTR^{P46P*}</i>	This study

Table 2.2 plasmids used in this study

Strain Number	Genotype	Source
DP-E6949	<i>pPL2-Phyper-hly</i>	Shen and Higgins
DP-E6950	<i>pPL2-Phyper-hly(TCT263AGC) S44S</i>	This study
DP-E6951	<i>pPL2-Phyper-hly(TCT263TCC) S44S</i>	This study
DP-E6952	<i>pPL2-Phyper-hly(TCT263TCA) S44S</i>	This study
DP-E6953	<i>pPL2-Phyper-hly(TCT263TCG) S44S</i>	This study
DP-E6954	<i>pPL2-Phyper-hly(TCT263AGT) S44S</i>	This study
DP-E6955	<i>pPL2-Phyper-hly(AAT233AAC) N34N</i>	This study
DP-E6956	<i>pPL2-Phyper-hly(TCA236TCG) S35S</i>	This study
DP-E6957	<i>pPL2-Phyper-hly(ATT239ATC) I36I</i>	This study
DP-E6958	<i>pPL2-Phyper-hly(TCA242TCG) S37S</i>	This study
DP-E6959	<i>pPL2-Phyper-hly(TCC245ACG) S38S</i>	This study
DP-E6960	<i>pPL2-Phyper-hly(GCA251GCG) A40A</i>	This study
DP-E6961	<i>Δhly pPL2-Phyper-hly(CCA254CCG) P41P</i>	This study
DP-E6962	<i>pPL2-Phyper-hly(CCA257CCG) P42P</i>	This study
DP-E6963	<i>pPL2-Phyper-hly(GCA260GCG) A43A</i>	This study
DP-E6964	<i>pPL2-Phyper-hly(GCG266CCC) P45P</i>	This study
DP-E6965	<i>pPL2-Phyper-hly(CCT269CCG) P46P*</i>	This study
DP-E6966	<i>pPL2-Phyper-hly(CCT269CCA) P46P</i>	This study
DP-E6967	<i>pPL2-Phyper-hly(GCA272GCC) A47A*</i>	This study
DP-E6968	<i>pPL2-Phyper-hly(GCA272GCT) A47A</i>	This study
DP-E6969	<i>pPL2-Phyper-hly(AGT275TCG) S48S</i>	This study
DP-E6970	<i>pPL2-Phyper-hly(CCT278CCG) P49P</i>	This study
DP-E6971	<i>pPL2-Phyper-hly(AAG281AAA) K50K</i>	This study
DP-E6972	<i>pPL2-Phyper-hly(ACG284ACC) T51T</i>	This study
DP-E6973	<i>pPL2-Phyper-hly(CCA287CCC) P52P</i>	This study
DP-E6974	<i>pPL2-Phyper-hly(ATC290ATT) I53I</i>	This study
DP-E6975	<i>pPL2-Phyper-hly(GAA293GAG) E54E</i>	This study
DP-E6976	<i>pPL2-Phyper-hly(AAG296AAA) K55K</i>	This study
DP-E6977	<i>pPL2-Phyper-hly(A116T) UTR^{P46P}</i>	This study
DP-E6978	<i>pPL2-Phyper-hly(A116C) UTR^{P46P*}</i>	This study
DP-E6979	<i>pPL2-Phyper-hly(A116T) UTR^{P46P}</i>	This study

DP-E6980	<i>pPL2-Phyper-hly(A116T/T271A) P46P/UTR^{P46P}</i>	This study
DP-E6981	<i>pPL2-Phyper-hly(A116C/T271G) P46P*/UTR^{P46P*}</i>	This study
DP-E6982	<i>pPL2-Phyper-hly(T113A) UTR^{A47A}</i>	This study
DP-E6983	<i>pPL2-Phyper-hly(T113G) UTR^{A47A*}</i>	This study
DP-E6984	<i>pPL2-Phyper-hly(U113A/A274T) A47A/UTR^{A47A}</i>	This study
DP-E6985	<i>pPL2-Phyper-hly(U113G/A274C) A47A*/UTR^{A47A*}</i>	This study
DP-E6986	<i>pPL2-Phyper-hly(A116T/A274T) A47A/UTR^{P46P}</i>	This study
DP-E6987	<i>pPL2-Phyper-hly(A116C/A274C) A47A*/UTR^{P46P*}</i>	This study
DP-E6988	<i>pPL2-Phyper-hly(T113A/T271A) P46P/UTR^{A47A}</i>	This study
DP-E6989	<i>pPL2-Phyper-hly(T113G/T271G) P46P*/UTR^{A47A*}</i>	This study
DP-E6990	<i>pKSV7 hly</i>	This study
DP-E6991	<i>pKSV7 hly(TCT263AGC) S44S</i>	This study
DP-E6992	<i>pKSV7 hly (AA111CT)</i>	This study
DP-E6993	<i>pKSV7 hly (AA111CT/ TCT263AGC) AA111CT/S44S</i>	This study
DP-E6994	<i>pKSV7 hly(CCT269CCA) P46P</i>	This study
DP-E6995	<i>pKSV7 hly(CCT269CCG) P46P*</i>	This study
DP-E6996	<i>pKSV7 hly(A116U) UTR^{P46P}</i>	This study
DP-E6997	<i>pKSV7 hly(A116C) UTR^{P46P*}</i>	This study
DP-E6998	<i>pKSV7 hly(A116U/U271A) P46P/UTR^{P46P}</i>	This study
DP-E6999	<i>pKSV7 hly(A116C/U271G) P46P*/UTR^{P46P*}</i>	This study

Table 2.3 oligonucleotides used in this study

Description	FWD	REV
<i>hly(TCT263AGC)</i> S44S	CATCCATGGCACCACCAGCA AGCCCGCCTGCAAG	CTTGCAGGCGGGCTTGCTGGTGGT GCCATGGATG
<i>hly(TCT263TCC)</i> S44S	CACCACCAGCATCCCCGCCT GCAAGTC	GACTTGCAGGCGGGGATGCTGGT GGTG
<i>hly(TCT263TCA)</i> S44S	GACTTGCAGGCGGTGATGCT GGTGGTG	CACCACCAGCATCACCGCCTGCAA GTC
<i>hly(TCT263TCG)</i> S44S	CACCACCAGCATCGCCGCCT GCAAGTC	GACTTGCAGGCGGCGATGCTGGT GGTG
<i>hly(TCT263AGT)</i> S44S	CCATGGCACCACCAGCAAG TCCGCCTGC	GCAGGCGGACTTGCTGGTGGTGCC ATGG
<i>hly(AAT233AAC)</i> N34N	AAAGGATGCATCTGCATTCA ATAAAGAAAACCAATTTC TCCATGGC	GCCATGGATGAAATTGAGTTTTCT TTATTGAATGCAGATGCATCCTTT
<i>hly(TCA236TCG)</i> S35S	CATCTGCATTCAATAAAGAA AATTCGATTTTCATCCATGGC ACCACC	GGTGGTGCCATGGATGAAATCGA ATTTTCTTTATTGAATGCAGATG
<i>hly(ATT239ATC)</i> I36I	GCATCTGCATTCAATAAAGA AAATTCATCTCATCCATGG CACCA	TGGTGCCATGGATGAGATTGAATT TTCTTTATTGAATGCAGATGC
<i>hly(TCA242TCG)</i> S37S	TGCATTCAATAAAGAAAATT CAATTCGTCCATGGCACCA CCAGC	GCTGGTGGTGCCATGGACGAAATT GAATTTTCTTTATTGAATGCA
<i>hly(TCC245ACG)</i> S38S	TGCATTCAATAAAGAAAATT CAATTTCAAGCATGGCACCA CCAGCATC	GATGCTGGTGGTGCCATGCTTGAA ATTGAATTTTCTTTATTGAATGCA
<i>hly(GCA251GCG)</i> A40A	CAATTTTCATCCATGGCGCCA CCAGCATCTCCGC	GCGGAGATGCTGGTGGCGCCATG GATGAAATTG
<i>hly(CCA254CCG)</i> P41P	CATCCATGGCACCAGCCAGCA TCTCCGC	GCGGAGATGCTGGCGGTGCCATG GATG
<i>hly(CCA257CCG)</i> P42P	CCATGGCACCACCGCATCT CCGCCTG	CAGGCGGAGATGCCGGTGGTGCC ATGG
<i>hly(GCA260GCG)</i> A43A	GGCACCACCAGCGTCTCCGC CTGCA	TGCAGGCGGAGACGCTGGTGGTG CC
<i>hly(GCG266CCC)</i> P45P	TTAGGACTTGACAGGGGGAG ATGCTGGTGG	CCACCAGCATCTCCCCCTGCAAGT CCTAA
<i>hly(CCT269CCG)</i> P46P*	CCAGCATCTCCGCCGGCAAG TCCTAAGAC	GTCTTAGGACTTGCCGGCGGAGAT GCTGG

<i>hly(CCT269CCA)</i> P46P	CACCACCAGCATCTCCGCCA GCAAGTCCTAAGACGCCAA T	ATTGGCGTCTTAGGACTTGCTGGC GGAGATGCTGGTGGTG
<i>hly(GCA272CCC)</i> A47A*	GGCGTCTTAGGACTGGCAG GCGGAGATGC	GCATCTCCGCCTGCCAGTCCTAAG ACGCC
<i>hly(GCA272CCT)</i> A47A	GCACCACCAGCATCTCCGCC TGCTAGTCCTAAGACGCCAA TCG	CGATTGGCGTCTTAGGACTAGCAG GCGGAGATGCTGGTGGTGC
<i>hly(AGT275TCG)</i> S48S	GATTGGCGTCTTAGGCGATG CAGGCGGAGATGCTGGT	ACCAGCATCTCCGCCTGCATCGCC TAAGACGCCAATC
<i>hly(CCT278CCG)</i> P49P	TCGATTGGCGTCTTCGGACT TGCAGGCGG	CCGCCTGCAAGTCCGAAGACGCC AATCGA
<i>hly(AAG281AAA)</i> K50K	CTCCGCCTGCAAGTCCTAAA ACGCCAATCGAA	TTCGATTGGCGTTTTAGGACTTGC AGGCGGAG
<i>hly(ACG284ACC)</i> T51T	CCTGCAAGTCCTAAGACCCC AATCGAAAAGAAACA	TGTTTCTTTTCGATTGGGGTCTTAG GACTTGCAGG
<i>hly(CCA287CCC)</i> P52P	GCAAGTCCTAAGACGCCCAT CGAAAAGAAACACGC	GCGTGTTCCTTTTCGATGGGCGTC TTAGGACTTGC
<i>hly(ATC290ATT)</i> I53I	AGTCCTAAGACGCCAATTGA AAAGAAACACGCGGA	TCCGCGTGTTCCTTTTCAATTGGC GTCTTAGGACT
<i>hly(GAA293GAG)</i> E54E	TCATCCGCGTGTTCCTTCTC GATTGGCGTCTTAGG	CCTAAGACGCCAATCGAGAAGAA ACACGCGGATGA
<i>hly(AAG296AAA)</i> K55K	CCTAAGACGCCAATCGAAA AAAAACACGCGGATGAAAT C	GATTTTCATCCGCGTGTTCCTTTTCG ATTGGCGTCTTAGG
<i>hly(A116U)</i> UTR ^{P46P}	ATTAGGTTAAAAAATGTTGA AGGAGAGTGAAACCCATGA AA	TTTCATGGGTTTCACTCTCCTTCAA CATTTTTTAACCTAAT
<i>hly(A116C)</i> UTR ^{P46P*}	GGTTAAAAAATGTCAAGG AGAGTAAA	TTTCACTCTCCTTCGACATTTTTTA ACC
<i>hly(U113A)</i> UTR ^{A47A}	TTATTAGGTTAAAAAAGTA GAAGGAGAGTGAAACCCA	TGGGTTTCACTCTCCTTCTACTTTT TTAACCTAATAA
<i>hly(U113G)</i> UTR ^{A47A*}	TTAGGTTAAAAAAGGTAGA AGGAGAGTG	CACTCTCCTTCTACCTTTTTTAACC TAA
<i>hly(AA111CT)</i>	TGGCATTATTAGGTTAAAAC TTGTAGAAGGAGAGTGAAA CCCAT	ATGGGTTTCACTCTCCTTCTACAA GTTTTAACCTAATAATGCCA
RNaseIII	ATGGGGTCCAGCGGCGCTG GATCCTGCGCCCCGTGGTAT	GCTCGCTCCACTGCCTCCTGCAGC TTTTCCGTTTCGACTAAAAGGC

<i>hly</i>KSV7	ATGGGGTCCAGCGGGCGCTG GATCCTGTAGGGATTTTATT GCTCGTGT	GCTGCAGGAGGCAGTGGAGCGAG CGGTTTCCGACATAACTTTTACA T
<i>hly</i>RT with TGIRT	ACCTGGATAGGTTAGGCTCG AAATTGCATTCACAACTT	-
<i>hly</i>_PCR	GCAAGCATATAATATTGCGT TTCATC	ATTGATGGATTTCTTCTTTTTCTCC A
<i>hly</i>qPCR	GTTCAAATCATCGACGGCAA CCTC	TTGAGCAACGTATCCTCCAGAGTG
23SqPCR	AGGATAGGGAATCGCACGA A	TTCGCGAGAAGCGGATTT

Chapter 3: CbpB activates the stringent response during low c-di-AMP conditions

Portions of this chapter are part of a manuscript in preparation:

Peterson BN, Young M, Wang J, Whiteley AT, Woodward JJ, Luo S, Tong L, Wang JD, Portnoy DA. CbpB is a c-di-AMP dependent activator of the stringent response in Firmicutes. *In preparation*

Introduction

Nucleotide second messenger molecules are ubiquitous and widely conserved throughout microbial life. Their structural diversity reflects their numerous functions within microbes *and* eukaryotic cells. The ever-expanding repertoire of nucleotide second messengers in bacteria highlights the complexity of their individual functions and interactions (50). Their pervasiveness suggests that multiple second messenger can exist within a single cell, opening the possibility of crosstalk with one another.

Guanosine tetra- and pentaphosphate (ppGpp and pppGpp) are two of the earliest discovered and best-studied nucleotide bacterial nucleotide second messengers(89). (p)ppGpp is synthesized in response to starvation and orchestrates the re-organization of cellular processes away from protein synthesis and ribosome biogenesis and towards the expression of genes involved in cell survival and metabolite production (90). This process is termed the “stringent response.” Induction of the stringent response has been best characterized in the context of amino acid starvation, which involves (p)ppGpp synthesis at a stalled ribosome by the bifunctional synthase/hydrolase enzyme, here called RelA (48). RelA is conserved across all bacteria, archaea and plant chloroplasts. Since the stringent response can be activated by conditions other than amino acid starvation, alternative induction pathways must exist but have yet to be fully elucidated (91-93).

cyclic-di-AMP is a more recently discovered nucleotide second messenger and is a member of the conspicuous cyclic di-nucleotides. It is involved in maintenance of cell envelope integrity, osmoregulation and the central metabolism of bacteria (53-55). Much attention has been bestowed on the cyclic di-nucleotide because of its ability to communicate across domains of life and interact with the metazoan immune system (52), which has highlighted its roles in the context of host-microbe interactions. In many organisms c-di-AMP is required for growth on rich media (56). Using a c-di-AMP-deficient strain of the facultative intracellular pathogen *Listeria monocytogenes*, it was recently shown that the essentiality of c-di-AMP was in part due to the toxic accumulation of (p)ppGpp (56). This result implied a connection in the signaling pathways of two critical second messengers. Though the relationship between c-di-AMP and (p)ppGpp is known, the molecular basis of this nucleotide cross talk has not been clear.

Here we find that the conserved c-di-AMP-binding protein, CbpB, serves as a molecular link between c-di-AMP signaling and the stringent response. *In vivo* analyses show that CbpB causes (p)ppGpp accumulation when c-di-AMP levels are low and that deleting *cbpB* in c-di-AMP deficient bacteria restores WT (p)ppGpp levels. Crystal structures reveal that CbpB binds to c-di-AMP as a homodimer and changes relatively little between bound and unbound states. We identify that RelA is a molecular target of CbpB and show that CbpB binds RelA and promotes (p)pppGpp accumulation in a c-di-AMP-dependent manner. These data build upon previous work detailing the relationship between the two signaling pathways and provide a novel example of non-canonical stringent response activation.

Results

Deletion of cbpB does not rescue cell wall defects in a $\Delta dacA$ background

We previously reported (53, 56, 94) that c-di-AMP-deficient ($\Delta dacA$) *L. monocytogenes* mutant was unable to grow on rich media, had cell envelope defects, and was avirulent in a mouse model of infection. We further showed that suppressor mutations could rescue growth on rich media and that genes that acquire mutations fall into several separate pathways, including osmolyte uptake (*oppABCDF* and *gbuABC*), central metabolism (*pycA* and *pstA*), and the stringent response (*relA*). Suppressor mutations were also identified in a gene of unknown function called cyclic di-AMP binding protein B (*cbpB*) and can be attributed to a loss-of-function phenotype, as deleting *cbpB* in $\Delta dacA$ bacteria allows for growth on rich media. We wanted to understand the contribution of CbpB to maintenance of cell integrity within the context of infection.

The intracellular niche of *Listeria* provides a unique environment to understand aspects of bacterial physiology and cell structure. We decided to use the host cell to measure the amount of bacteriolysis from our $\Delta dacA\Delta cbpB$ mutant by measuring the amount of AIM2-dependent cytotoxicity in murine bone marrow macrophages. AIM2 is a cytosolic DNA sensor that, when activated, will cause Caspase-1-mediated pyroptosis (95). Infections of B6 macrophages resulted in comparable cytotoxicity levels across WT, $\Delta dacA$ and $\Delta dacA\Delta cbpB$ strains (Fig. 3.1A); however, when infections were performed in AIM2^{-/-} macrophages, there was a significant reduction of cell death in $\Delta dacA$ and $\Delta dacA\Delta cbpB$ -infected cells (Fig. 3.1B), indicating a release of bacterial DNA into the macrophage cytoplasm.

A complementary way to examine cytosolic DNA release is to measure type-1 interferon production. In WT-infected macrophages, type-1 interferon is expressed due to actively secreted cyclic di-AMP binding STING. This pathway is also activated by cyclic GMP-AMP synthase (cGAS) binding to cytosolic DNA. We found that type-1 interferon induction was much lower in cGAS^{-/-} macrophages infected with $\Delta dacA$ or $\Delta dacA\Delta cbpB$ bacteria compared to WT, indicating comparable levels of DNA release for these two mutants (Fig. 3.1C,D). These data indicate that the role of CbpB is not directly related to bacterial integrity.

In a mouse model of infection, deleting *cbpB* did not restore any of the virulence defect caused by the lack of c-di-AMP (Fig. 3.1E). This indicated the *cbpB* was not involved in any cell envelope defects in the $\Delta dacA$ background despite suppressing the essentiality of c-di-AMP on rich media.

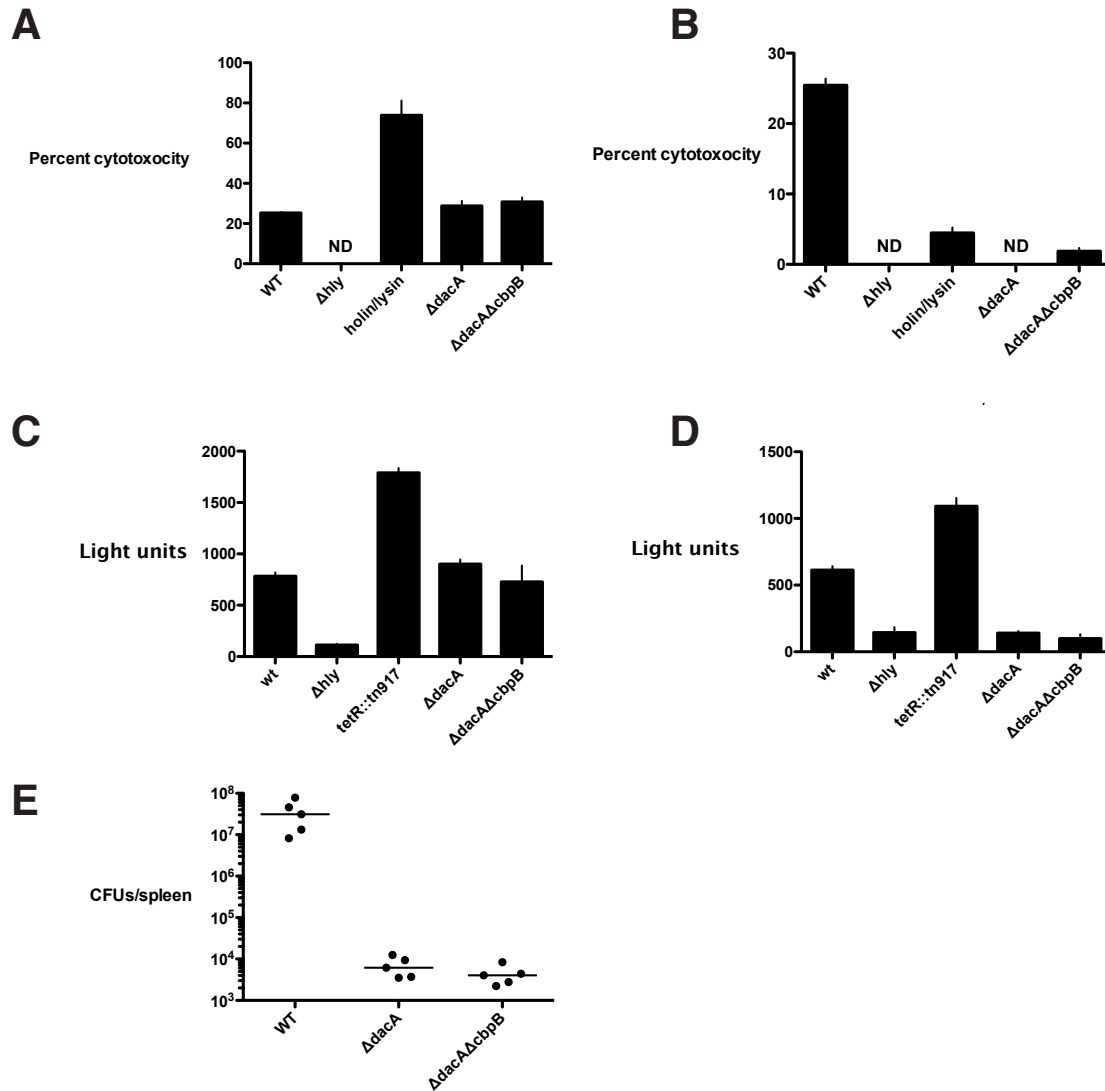


Figure 3.1. CbpB does not affect cell envelope defect in Δ dacA mutants.

LDH release assay showing the cytotoxicity caused by *L. monocytogenes* mutants in B6 (A) and *Aim2*^{-/-} (B) macrophages. (C) ISRE results showing type I interferon signaling in B6 macrophages and *cGAS*^{-/-} (D) macrophages. (E) Mouse model of infection (iv). ND = not detected.

CbpB is toxic to bacteria deficient in *c-di-AMP*

Because *cbpB* expression is toxic to Δ dacA cells grown in rich media, we reasoned that manipulating CbpB levels in this background on *Listeria* synthetic media (LSM, normally permissive for Δ dacA bacteria) could facilitate identification of its role in c-di-AMP signaling. Consistent with CbpB being toxic in the absence of c-di-AMP, standard attempts to construct a strain expressing *cbpB* in a Δ dacA background were unsuccessful. We thus developed a cre-lox-based approach to generate a *dacA* deletion strain while over-expressing *cbpB* (*dacA*^{fl} *cre-cbpB*) (Fig. 3.2A). This strain expresses the *cre* recombinase under the control of the inducible *actA* promoter. Infection of bone marrow macrophages with this strain resulted in extremely low recovery of bacteria on LSM compared to a train that encoded only the endogenous *cbpB*,

indicating that CbpB was rendering these bacteria unable to grow (Fig. 3.2B). Induction of *dacA* deletion *in vitro* by activation of *actA* transcription resulted in a plating deficiency (Fig. 3.2C). Consistent with this being the result of a lack of c-di-AMP, complementation with *dacA* or the *B. subtilis* paralog *disA* rescued this phenotype.

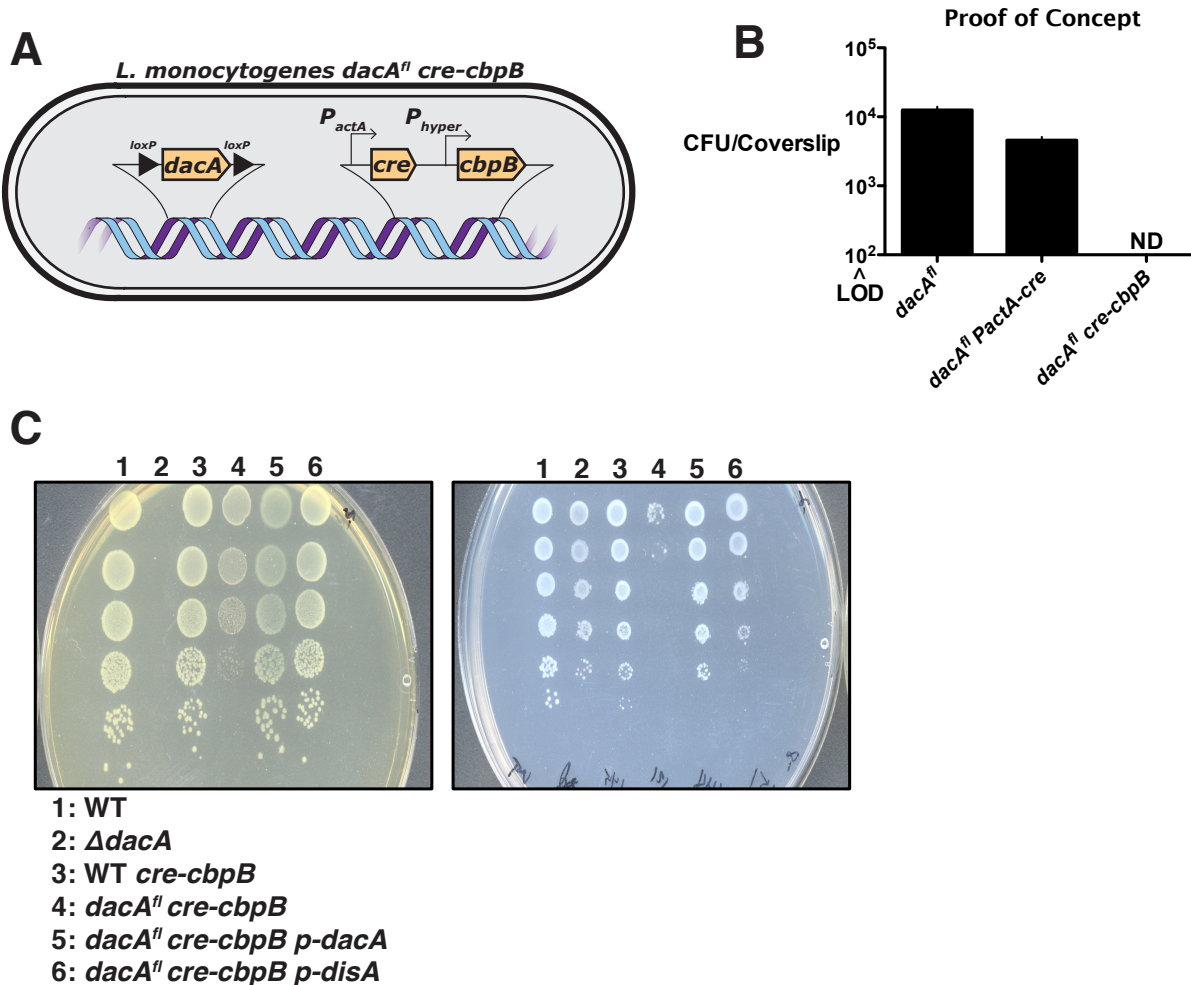


Figure 3.2. CbpB is toxic in the absence of c-di-AMP

(A) Construction of a strain to test CbpB function. *dacA^{fl} cre-cbpB* was engineered to flox the *dacA* genes while constitutively expressing *cbpB*. (B) Infection of BMMs with *dacA^{fl} cre-cbpB* resulted in extremely low recovery of bacteria after 4-hour infection. (C) Plating this strain on *actA*-activating media resulted in a plating deficiency, which was restored by the addition of *Lm dacA* or *B. subtilis disA*.

CbpB expression in the absence of cyclic di-AMP results in induction of the stringent response

While deletion of *dacA* in the CbpB-overexpressing strain resulted in a drastic decrease in recovered colony-forming units, we hypothesized that the few colonies that did grow contained mutations that would provide insight into *cbpB* function. We sequenced the genomes of 25 separately isolated suppressor strains. Consistent with CbpB being toxic in absence of *dacA*, analysis of the sequencing results revealed that the majority of strains had non-synonymous SNPs in *cbpB* (Table 3.1). We additionally identified multiple suppressor strains

with mutations in the synthase domain of the bifunctional (p)ppGpp synthase/hydrolase enzyme RelA (Fig. 3.3A). This suggested that (p)ppGpp toxicity was the cause of the bacterial growth inhibition.

Stringent response induction is a known reason for *dacA* essentiality on rich media. A previously characterized RelA synthase mutant (R295S), which was impaired for (p)ppGpp production, was recombined into our *dacA^{fl} cre-cbpB* strain and rescued growth on *actA*-activating media (Fig. 3.3B).

To directly test induction of the stringent response in our strain we quantified the ratio of (p)ppGpp/(p)ppGpp + GTP in *dacA^{fl} cre-cbpB* from phosphate limiting LSM. The *dacA^{fl} cre-cbpB* strain produced higher levels of (p)ppGpp than WT and *dacA^{fl} cre* (Fig. 3.3C, D). Although the *dacA^{fl} cre-cbpB* strain in this case is not depleted for c-di-AMP, we know it to produce lower levels of the di-nucleotide due to the placement of the *loxP* site 5' to *dacA* (Data not shown).

If alarmone production in cyclic di-AMP-depleted bacteria is driven by CbpB expression, then (p)ppGpp levels in $\Delta dacA \Delta cbpB$ should not be affected. When bacteria were grown in phosphate starved media lacking tryptone (to allow for $\Delta dacA$ growth) $\Delta dacA \Delta cbpB$ produced WT level alarmone levels (Fig. 3.3E). Interestingly, $\Delta dacA \Delta oppB$ and $\Delta dacA \Delta pstA$ strains (double mutants that also suppress *dacA* essentiality) produced $\Delta dacA$ levels of alarmone; suggesting that the nature of these suppressor mutations, with respect to their role in rescuing *dacA* essentiality, is differ from *cbpB*. Taken together, these data show that there is a direct link between CbpB expression and the stringent response in bacteria with low or no cyclic di-AMP.

Gene	Protein	No. times hit (distinct)	Non-synonomous
Imo1009	CbpB	10 (10)	Yes
Imo1523	RelA	2 (2)	Yes
Imo1296	HflX (GTPase)	4 (1)	Yes
Imo0389	LtrA (Low Temp requirement protein)	1	Yes
Imo0456	Hypothetical (putative cytosine permease)	1	Yes
Imo0587	Hypothetical (secreted)	1	Yes
Imo1904	BirA (transcriptional repressor)	1	Yes
Imo2188	Oligoendopeptidase	1	Yes
Imo2440	Hypothetical (endonuclease)	1	Yes

Table 3.1 SNPs identified from suppressor screen

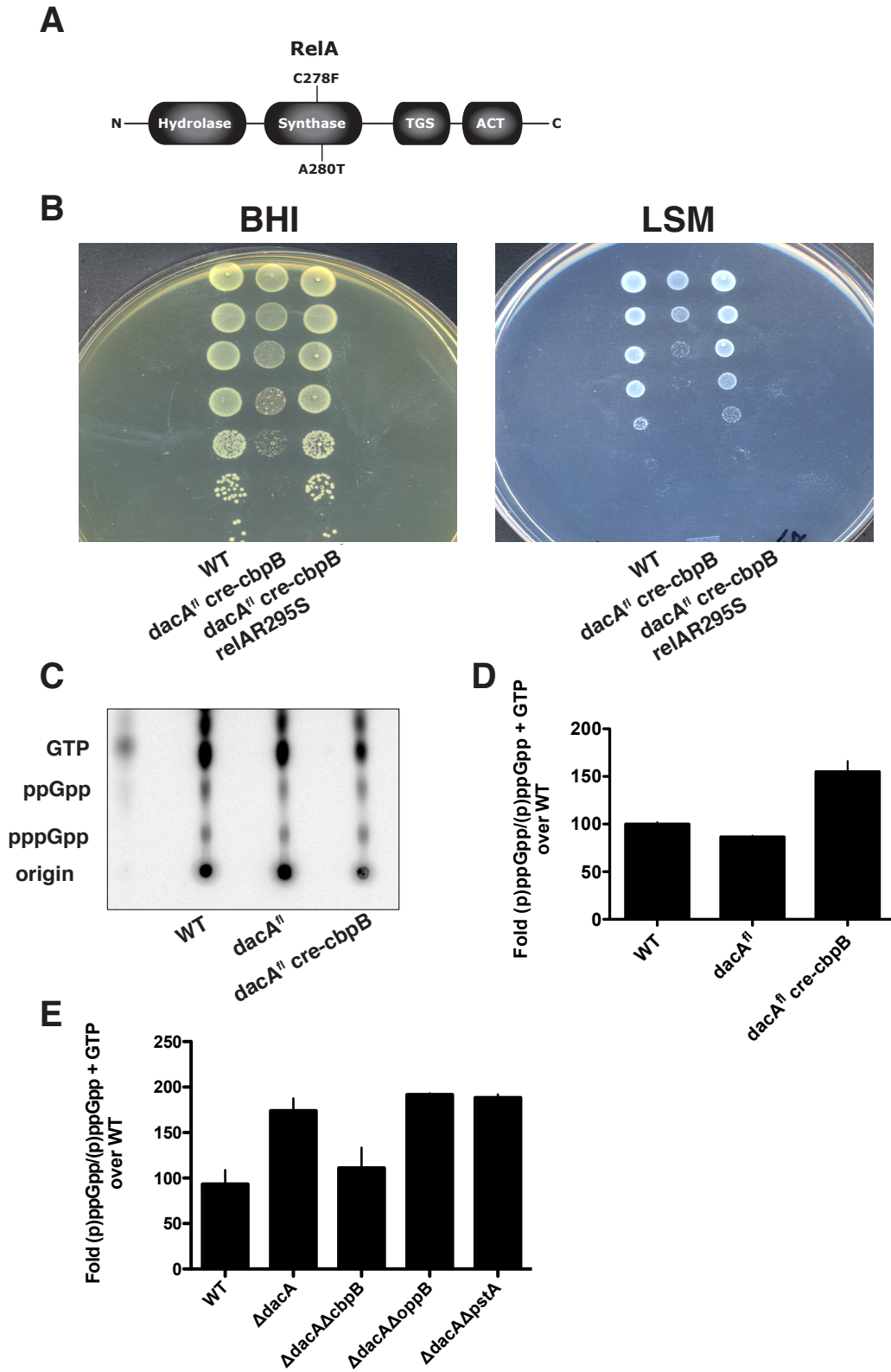


Figure 3.3. CbpB induces the stringent response in the absence of c-di-AMP

(A) mutations in RelA that were identified from genomic sequencing analysis. (B) Transduction of a synthase-dead mutant into *dacA^{fl}cre-cbpB* rescues growth on *actA*-activating media. (C) TLC of (p)ppGpp and GTP with

quantification (D) showing that CbpB induces the stringent response during c-di-AMP depleted conditions. (E) Deletion in *cbpB* restores $\Delta dacA$ (p)ppGpp levels to WT. Deletions in *pstA* and *oppB* (which also suppress *dacA* essentiality) do not affect alarmone levels, indicating alternative pathways of maintaining c-di-AMP essentiality.

Binding mode of c-di-AMP to CbpB

The CbpB protein consists of a two CBS domains and was previously shown to bind c-di-AMP. To gain insight into how c-di-AMP could influence CbpB function, we determined the structures of free CbpB and its complex with c-di-AMP at 1.6 and 2.4 Å resolution, respectively (Table 3.3). These structures reveal that CbpB has tandem CBS domains (CBS1 and CBS2) that interact to form a disk-like head-to-head homodimer. In the c-di-AMP complex, one U-shaped c-di-AMP molecule is bound to each face of the disk (Figs. 3.4A, B). One of the adenine bases of c-di-AMP is located in the cleft between the two tandem CBS domains (CBS1 and CBS2) of each monomer, while the other is projected into the solvent.

Specific recognition of c-di-AMP is achieved by a large number of hydrogen bonds with both main chains and side chains of CbpB, some of which are mediated by water molecules. The adenine base in the cleft is recognized through hydrogen bonds to its N1 and N6 atoms (Fig. 3.4C). It is π -stacked against Tyr45 on one face while its other face is flanked by Ile19 and Ile128, thereby forming a narrow pocket for the binding of this base. Its ribose is positioned against the side chain of Phe115, and the 2' hydroxyl group has hydrogen-bonding interactions with the main chain of Val47. The 5' phosphate is recognized by hydrogen-bonding interactions with the main-chain amide of Arg131, ionic interactions with Arg132 from the other monomer, and hydrogen-bonding interactions with the side-chain amide of Thr130 through a water molecule. This phosphate is situated in a generally positively-charged region of the structure.

In contrast, the other adenine base of c-di-AMP has no hydrogen-bonding interactions with CbpB, and it is not flanked by residues from the protein either, except that its N6 atom is positioned against Tyr45 (Fig. 3.4C). The 2' hydroxyl group of its ribose has hydrogen-bonding interactions with the side chain of Arg131 from the other monomer. The 5' phosphate has hydrogen-bonding interactions with the main chain and side chain of Ser46. One of the terminal oxygen atoms on this phosphate is 4.4 Å away from the equivalent atom in the c-di-AMP molecule on the other face of the disk (Fig. 3.4B).

This binding site of c-di-AMP, especially Tyr45 and the residues flanking the adenine on the other face, is well conserved among CbpB homologs (Fig. 3.4D). This analysis reveals another conserved surface patch, located away from the c-di-AMP binding site and formed by residues in CBS1, which may mediate a separate function of this protein.

The overall structure of free CbpB is similar to the c-di-AMP complex, with rms distance of 0.86 Å between their equivalent C α atoms (Fig. 3.4E). However, there are important structural differences in the c-di-AMP binding site. Especially, the conformation of Tyr49 side chain has severe clashes with the bound position of c-di-AMP (Fig. 3.4F), and therefore the binding site does not exist in free CbpB.

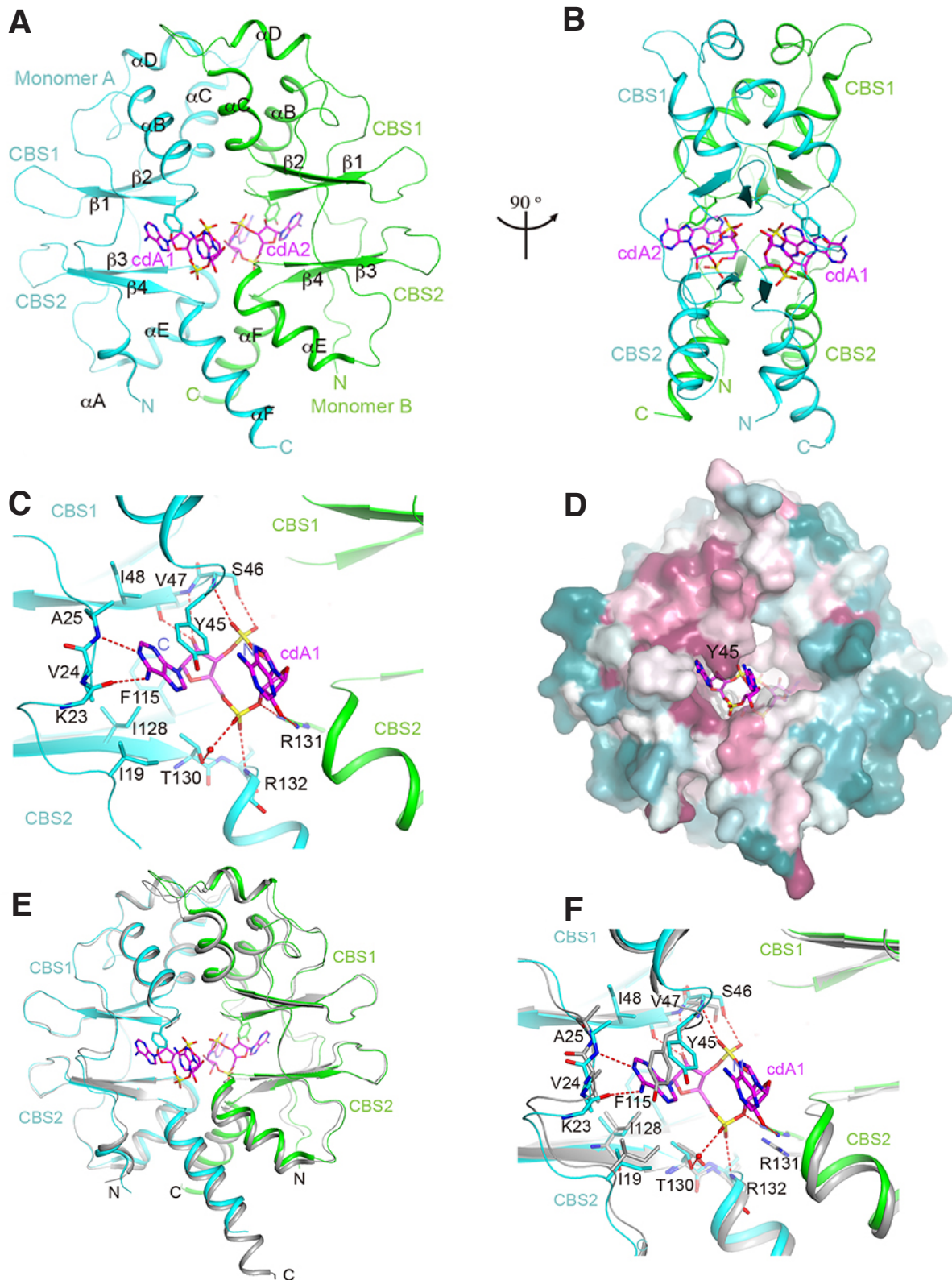


Figure 3.4. Crystal structure of CbpB in complex with c-di-AMP

(A). Overall structure of the CbpB homodimer (monomer A in cyan, monomer B in green) in complex with c-di-AMP (labeled cdA1 and cdA2, carbon atoms colored magenta, blue for nitrogens, yellow for phosphorus, and red

for oxygens). The two tandem CBS domains in each monomer are labeled CBS1 and CBS2. Helices and strands in the two monomers are also labeled. **B**). Overall structure of the CbpB homodimer in complex with c-di-AMP, after a 90° rotation around the vertical axis. **C**). Detailed interactions between CbpB and c-di-AMP. Hydrogen bonds and water molecule are shown with red dashed lines and red sphere. Residues involved in interaction are also labeled. The side chains of Arg132 and Lys32 are not shown for clarity. **D**) Sequence conservation of CbpB homologs, generated by the program ConSurf (Armon et al., 2001) based on an alignment of 150 sequences selected automatically. Purple indicates conserved residues, cyan indicates variable residues, and white indicates average conservation. Molecular surface of CbpB near the binding sites for c-di-AMP, colored according to the electrostatic potential (blue: positive, red: negative). **E**) Overlay of the structure of the CbpB homodimer (monomer A in cyan, monomer B in green) in complex with c-di-AMP (magenta) with that of free Lmo1009 (gray). **B**) Structural differences in the binding site for c-di-AMP in free CbpB. The side chains of Arg132 and Lys32 are not shown for clarity.

CbpB interacts with and activates the synthase region of RelA

We hypothesized that CbpB could be localizing with RelA at the ribosome to activate the stringent response. After multiple failed attempts to locate CbpB within polysomal fractions we decided on an unbiased Yeast Two Hybrid (Y2H) screen to search for interacting *Listeria* proteins. Surprisingly, the most common prey construct identified on the highly stringent QDO/X/A (see experimental procedures) was a fragment of the synthase domain of RelA (Table 3.2). This prey plasmid was purified from the yeast and its interaction with CbpB was verified by measuring the α -galactosidase activity (Fig. 3.5A). The full length RelA construct produced minimal α -gal but allowed for a small amount of growth on the high stringency plates (Fig. 3.5B), suggesting a reduced interaction or improper protein folding in yeast.

To better understand the nature of the interaction, the effect of CbpB on synthesis and hydrolysis of (p)ppGpp by RelA were tested *in vitro*. RelA-His was kept at a concentration of 1.15 μ M and CbpB and cyclic-di-AMP were tested at concentrations of 2.3 μ M and 4.6 μ M. In the control reaction, RelA hydrolysis activity occurs at a faster rate than its synthesis activity. Addition of CbpB increased the rate of pppGpp synthesis (Fig. 3.5D) and decreased the rate of hydrolysis (Fig. 3.5C). Addition of cyclic-di-AMP to this reaction reverted RelA synthesis and hydrolysis activities to levels similar to RelA in the absence of CbpB. On its own, cyclic-di-AMP had no effect on RelA activities (data not shown). These results suggest that the CbpB interaction with the RelA synthase domain activates synthesis (and/or inhibits hydrolysis).

These data indicate that CbpB interacts with RelA and regulated its enzymatic function. Further work with synthase/hydrolase RelA mutants will elucidate the exact mechanism of influence CbpB imparts on RelA.

Table 3.2 Positive interacting proteins identified through YTH

Gene	Protein	No. times hit
Imo 1523	RelA	14
Imo 1079	Unknown	7
Imo 1357	Acetyl-CoA carboxylase	4
Imo 2654	Fus (translation elongation factor G)	3
Imo 0537	allantoate amidohydrolase	2
Imo 2196	Unknown protein	2
Imo 1811	Unknown protein	1
Imo 2438	Unknown protein	1
Imo 2051	Unknown protein	1
Imo 0911	Unknown protein	1
Imo 0842	Peptidoglycan bound protein	1

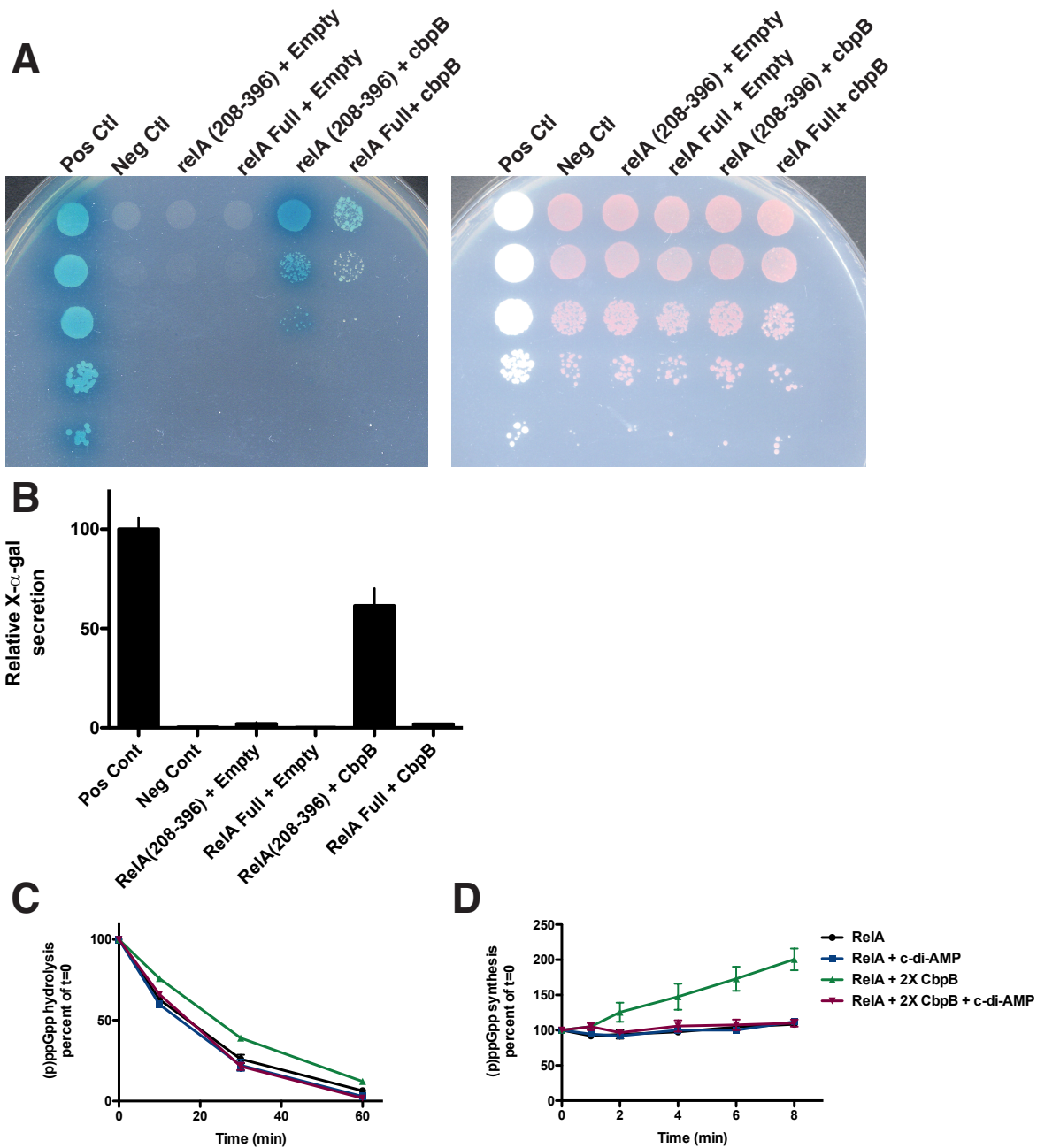


Figure 3.5. CbpB interacts with RelA and leads to increased (p)ppGpp

(A) Confirmation of YTH results showed that RelA can interact with CbpB. Left- QDO/X/A media only allows for growth when subunits are interacting. Right- DDO media allows for growth when yeast carry both prey and bait plasmids are present. See experimental procedures. (B) Quantification of X- α -gal activity. (C) Analysis of RelA hydrolase activity in the presence of CbpB, c-di-AMP or both. Error bars represent the range of 2 replicates. (D) RelA synthase activity in the presence of CbpB, c-di-AMP or both. Error bars represent the range of 2 replicates

Discussion

Here, we describe a novel non-canonical mechanism of stringent response induction. We show that c-di-AMP inhibits the stringent response through the expression of *cbpB* and that deleting *cbpB* in mutants lacking c-di-AMP restores normal alarmone levels. CbpB binds directly to RelA in the absence of c-di-AMP and leads to the toxic accumulation of (p)ppGpp. The crystal structure of c-di-AMP with CbpB shows that they bind in a 1:1 ratio, with CbpB forming only a small conformational change between bound and unbound states.

The stringent response is induced by a variety of starvation conditions (carbon, nitrogen, fatty acid, phosphate and iron) as well as cell envelope stress. It has become increasingly clear in recent years that the ability to respond to disparate stresses is achieved through multiple non-canonical activation mechanisms. In *E. coli*, RSD and Acyl-carrier protein bind SpoT (a RelA homolog) during carbon and lipid starvation, respectively, and induce opposing hydrolase or synthase activities (91, 93). In *C. crescentus*, EII^{NTR}~P can bind SpoT in response to nitrogen starvation and activate the hydrolase domain (96). In multiple bacterial phyla, branched chain amino acids bind to RelA and regulate (p)ppGpp hydrolysis (92). These mechanisms offer a direct link between a specific stress and the cellular response.

While the stringent response seems to allow for a general adaptation to multiple stresses, the physiological role of c-di-AMP signaling remains more ambiguous. The relationships between c-di-AMP and (p)ppGpp is complex. While depletion of c-di-AMP leads to stringent activation, over-production of the cyclic di-nucleotide induces the same response in *S. aureus*(57). Though the molecular mechanism for high c-di-AMP stringent activity has not been elucidated, it is unclear if *S. aureus* contains a definitive *cbpB* homolog (see below) (55). (p)ppGpp also inhibits the activity of two mechanistically distinct phosphodiesterases in *L. monocytogenes* that are responsible for c-di-AMP degradation; PdeA (a DHH-DHHA1 domain-containing enzyme homologous to GdpP) and PgpH (an HD-domain containing enzyme) (57, 58, 97). This suggests that a feedback loop exists between c-di-AMP and (p)ppGpp, wherein low c-di-AMP induces the stringent response through CbpB, and the consequence of this is increase of cellular c-di-AMP levels through the inactivation of phosphodiesterase activity.

The implication of the CbpB-RelA interaction is that two conditions must be satisfied for the stringent response: 1) c-di-AMP levels must be low enough to free CbpB to bind RelA, 2) CbpB must be synthesized. The genomic context of *cbpB* provides a clue into when and why it is expressed. *cbpB* is normally found in an operon with a LysR-type transcriptional regulator known as *ccpC* (Supplementary genome structure). CcpC can bind citrate and regulate genes in the oxidative branch of the tricarboxylic acid (TCA) cycle resulting in regulation of the genes involved in carbon flow through this pathway, as well as autoregulation of its own operon (98-101). In *L. monocytogenes* there is no TCA cycle, however this branch is intact presumably for metabolite biosynthesis. Regulation of citrate production in *L. monocytogenes* is of particular concern for *AdacA* mutants, which are susceptible to its toxic effects (53). Accordingly, c-di-AMP regulates carbon flow through this pathway through the allosteric inhibition of pyruvate carboxylase (PycA), which inhibits production of downstream metabolites, including citrate (54). It also binds to PstA, a protein of unknown function that can also regulate citrate production (53). CbpB does not affect citrate production in *AdacA* mutants, suggesting that its function is not to regulate carbon flux (Supplementary). Though we do not know when the oxidative TCA pathway is used in *L. monocytogenes* this mechanism links c-di-AMP with the generation of reducing equivalents in organisms with intact TCA cycles. Of note, the *ccpC* homolog in *S. aureus* (*ccpE*) is not in an operon with a stand-alone CBS domain-containing protein. This along

with the high c-di-AMP stringent activation suggests that the relationship between (p)ppGpp and c-di-AMP is different than in *L. monocytogenes*, (102, 103).

c-di-AMP signaling affects many different aspects of bacterial physiology. Its essentiality on rich media may only represent the most phenotypically severe stretches of its signaling networks. Our data indicate a model for how CbpB regulates the stringent response to protect the cell against the build-up of the toxic metabolite citrate when c-di-AMP levels are dangerously low. The work highlights the importance of the (p)ppGpp as a protective molecule against cell envelope stress and adds complexity to the relationship between metabolite production and starvation.

Experimental Procedures

Bacterial culture conditions

The *L. monocytogenes* strains used in this study (Table 3.4) were derived from wild-type 10403S were maintained in brain heart infusion (BHI, Difco) for *dacA*⁺ strains, and were maintained on Listeria synthetic media (LSM) for *dacA*-strains, in 1–3 ml of media in 14 ml (17 × 100 mm) culture tubes, at 37°C while shaking at 220 rpm, unless specified otherwise.

Listeria synthetic medium

The LSM was made using a previously described recipe (53). LSM was prepared by combining eight individual concentrated stock solutions (prepared ahead of time and stored at 4°C) with fresh glutamine and cysteine, see Supporting Information Table S1. Stock solutions were filter sterilized and stored at 4°C, with the exception of MOPS, Glucose and Phosphate which were stored at room temperature. Each stock was added at the appropriate dilution factor and in the order listed in Supporting Information Table S1, dissolving glutamine and cysteine immediately prior to filter sterilization. The final LSM is stable at 2× concentration and for approximately 6–8 weeks. LSM-agar plates are prepared by combining stock solutions with the fresh ingredients to a final 2× concentration, filter-sterilized, warmed to 37°C, combined with an equal volume of molten autoclave-sterilized 2× agarose (10 g l⁻¹ at 1×) and poured at 15 ml/plate. Agarose must be used, not agar, which is not sufficiently pure. It is recommended that the LSM-agarose be kept warm (> 55°C) while preparing the plates. *actA* activating media was made using LSM with the addition of 2mM 2-mercaptoethanol (BME) as previously described (104).

Mouse infections

8-week-old CD-1 outbred mice (Charles River) were infected intravenously with 1 × 10⁵ CFUs in 200 μl of PBS. Animals were sacrificed at 48 hours and spleens and livers were harvested in 5 ml or 10 ml in 0.1% IGEPAL CA-630 (Sigma) in water, respectively, and plated for enumeration of bacterial burdens.

Suppressor generation and identification

Briefly, mutants were cultured overnight in 5 ml of BHI and genomic DNA was extracted (MasterPure Gram Positive DNA Purification Kit, Epicentre) according to manufacturer's instructions. gDNA was then submitted for library preparation and Illumina sequencing (75PE MiSeq) at the UC Berkeley QB3 Genomics Sequencing Laboratory using. Data was assembled and aligned to the 10403S reference genome (GenBank: GCA_000168695.2) demonstrating > 50× coverage. SNP/InDel/structural variations from the wild-type strain were determined (CLC Genomics Workbench, CLC bio).

(p)ppGpp quantification

(p)ppGpp was measured as previously described with minor changes (56, 105). Bacteria were grown in low-phosphate listeria synthetic medium (LPLSM) (53). The *dacA*^{fl} *cre-cbpB* strain and other compared strains required growth in 1% Bacto-tryptone to inhibit spontaneous *actA* activation. Bacterial overnight cultures were diluted into LPLSM and grown for 2 to 5 h before re-suspending 5 × 10⁸ bacteria into 100 μl of either LPLSM or LPLSM plus 1% Bacto-tryptone with 20 μCi/ml carrier-free H₃³²PO₄. These cultures were incubated for 120 min at 37°C before resuspending in 50 μl of 13 M formic acid and freeze-thawing 4 times in a dry ice-ethanol bath

to lyse the cells. When utilized, serine hydroxamate was added at a concentration of 2 mg/ml for the final 15 min before harvest. Cell debris was removed by centrifugation, and extracts were spotted onto polyethyleneimine (PEI) cellulose thin-layer chromatography (TLC) plates (EMD Millipore) and developed in 1.5 M KH₂PO₄, pH 3.4. Dried TLC plates were exposed to phosphor-storage screens (Kodak) for >4 h before imaging on a Typhoon scanner (GE Healthcare). Nucleotides were identified using [γ -³²P]GTP and *E. coli* wild-type standard CF1943 (W3110 parental strain), which was generously provided by Michael Cashel (National Institutes of Health). The phosphor-storage screen scan results were quantified using ImageJ software (National Institutes of Health) without background subtraction. The volumes of intensity (without background correction) for identified nucleotide spots were used for calculation of (p)ppGpp levels as follows: (pppGpp + ppGpp) / (pppGpp + ppGpp + GTP).

Yeast 2 Hybrid

The Matchmaker Gold Yeast Two-Hybrid System (Clontech) was used to identify the interaction between CbpB and *Lm* proteins. CbpB was cloned into the pGBKT7 vector (Clontech) by Gibson assembly to generate pGBKT7-CbpB as the bait, then transformed into Y2HGold Competent Cells. The prey library was constructed from *L. monocytogenes* genomic DNA and consisted of >100,000 unique 1kb fragments. Full length RelA was inserted into the pGADT7 vector (Clontech) by Gibson assembly to generate pGADT7-RelA as the prey to confirm the interaction. *S. cerevisiae* containing pGBKT7-53 and pGADT7-T plasmids was used as a positive control, and *S. cerevisiae* containing pGBKT7-lam + pGADT7-T plasmids was used as a negative control. Plasmids were transformed into Y2HGold Competent Cells according to the small-scale transformation and mating procedure described in the Matchmaker Gold Yeast Two-Hybrid System user manual (Clontech). The Y2HGold bait strain and Y187 prey strain were mated in 2xYPDA and plated on SD/-Leu/-Trp/ (DDO) or SD/-Ade/-His/-Leu/-Trp/X-a-Gal/Aureobasidin A (QDO/X/A) agar plate. The activity of the secreted α -galactosidase enzyme was measured according to manufacturer's instructions (Clontech). Briefly, diploid *S. cerevisiae* strains were cultured in DDO medium and supernatants were collected from the overnight culture (20 hours post inoculation) and mixed with PNP- α -Gal Solution (Clontech). The reaction was terminated after 3 hours of incubation and optical density at 410nm was measured by SPECTRAMax (Molecular Devices).

Protein expression and purification

The gene encoding the CbpB protein (amino acid 1-150) was cloned into a modified pET28a plasmid to generate an N-terminal 6xHis-tagged protein. The construct was transformed into *E. coli* strain BL21 Star (DE3). Cells were grown at 37 °C with shaking vigorously at 250 rpm until the OD₆₀₀ reached 0.8 when they were induced by adding 0.4 mM isopropyl β -D-1-thiogalactopyranoside. Culture was further incubated at 25 °C for 12 hours and harvested by centrifugation. The cell pellet was resuspended using lysis buffer P500 containing 50 mM phosphate (pH 7.6), 500 mM NaCl, 20 mM imidazole and lysed by sonication. The lysate was cleared by high-speed centrifugation and the supernatant was incubated with Ni-NTA beads. Beads were washed by lysis buffer and protein was eluted using lysis buffer supplemented with 250 mM imidazole. The protein was further purified by gel filtration on Hiprep 16/60 Sepharyl 300 column (GE Healthcare) using a buffer containing 5 mM HEPES (pH 7.6), 200 mM NaCl and 2 mM DTT. The peak fractions containing pure CbpB which was confirmed by SDS-PAGE, were collected

and concentrated to 44 mg/ml. Protein was then flash frozen in liquid nitrogen and stored at -80°C .

Protein purification for RelA activity experiments

relA and *cbpB* were cloned into pET20b expression vectors. Protein was purified from Rosetta 2 cells as stated above.

Protein crystallization and structure determination

CbpB protein and its mixture with ATP or cyclic-di-AMP were all used for crystallization screening. Free CbpB crystals were grown within 2 days using the sitting-drop vapor-diffusion method at 20°C by mixing 15 mg/mL protein with equal volume of crystallization buffer containing 100 mM MES (pH 6.1) and 17% (v/v) MPD. Free CbpB structure was also observed using protein supplemented with 4 mM ATP in the same condition. Crystals were cryoprotected using 100 % Paratone[®] oil (Hampton research) and flash frozen in liquid nitrogen. X-ray diffraction data at 1.6 Å resolution were collected at Advanced Light Source (ALS) and processed using HKL2000 (106). The crystal belongs to space group $P2_12_12_1$ and each asymmetric unit contains a homodimer.

Crystals of CbpB in complex with cyclic-di-AMP were grown using the same method but in a different buffer condition, containing 100 mM imidazole (pH 8.0), 14% (w/v) PEG 8,000 and 200 mM CaCl_2 . Crystals were frozen using the same method. Data collection was performed at Advanced Photon Source (APS) and processed using HKL2000. The crystal diffracted to 2.4 Å resolution and belongs to the space group $P4_32_12$, with each asymmetric unit containing a homodimer.

The structure of free CbpB was solved by the molecular replacement method with Phaser (McCoy et al., 2007) as implemented in PHENIX (107), using the PDB entry 3LQN as the model (60% amino acid identity). The structure was refined with phenix.refine and manual adjustment was carried out with Coot (108). The structure in complex with cyclic-di-AMP was determined by molecular replacement using the structure of free Lmo1009 as the model and refined using phenix.refine. Strong density for the ligand was observed in the electron density map. The crystallographic information is summarized in Table 3.3.

Table 3.3 Summary of data collection and refinement statistics

	CbpB (apo)	CbpB-cdA complex
Data collection	ALS	APS
Space group	<i>P</i> 2 ₁ 2 ₁ 2 ₁	<i>P</i> 4 ₃ 2 ₁ 2
Cell dimensions		
<i>a</i> , <i>b</i> , <i>c</i> (Å)	54.26, 71.97, 74.65	61.93, 61.93, 171.51
α , β , γ (°)	90, 90, 90	90, 90, 90
Resolution (Å)*	43.3-1.6 (1.68-1.6)	24.9-2.4 (2.49-2.4)
<i>R</i> _{merge} (%)	4.6 (39.1)	7.7 (27.4)
CC _{1/2}	(0.91)	(0.83)
<i>I</i> / σ <i>I</i>	48.9 (2.4)	18.9 (2.6)
Completeness (%)	98.9 (90.8)	98.3 (92.9)
Redundancy	5.3 (4.3)	4.7 (4.2)
Refinement		
No. reflections	37576 (3514)	13573 (1249)
<i>R</i> _{work} (%)	20.2 (25.7)	21.3 (29.2)
<i>R</i> _{free} (%)	22.3 (27.3)	27.1 (39.1)
No. atoms		
Protein	2136	2120
Ligand/ion	1	90
Water	158	16
B-factors		
Protein	34.1	66.2
Ligand/ion	30.3	54.3
Water	40.3	61.8
R.m.s deviations		
Bond lengths (Å)	0.005	0.008
Bond angles (°)	0.72	0.91
Ramachandran statistics		
Favored (%)	99.23	98.85
Allowed (%)	0.77	1.15
Outliers (%)	0.00	0.00

*Values for highest resolution shell are shown in parentheses.

Table 3.4 *Lm* strains used in this study

Strain Number	Genotype	Source
DP-L184	10403S	(88)
DP-L6325	<i>ΔdacA</i>	(56)
DP-L7126	10403S <i>pPL2e PactA-cre Phyper-cbpB</i> (WT <i>cre-cbpB</i>)	This study
DP-L6254	<i>dacA^{fl}</i>	(56)
DP-L7127	<i>dacA^{fl} pPL2e PactA-cre</i> (<i>dacA^{fl} cre</i>)	This study
DP-L7128	<i>dacA^{fl} pPL2e PactA-cre Phyper-cbpB</i> (<i>dacA^{fl} cre-cbpB</i>)	This study
DP-L7129	<i>dacA^{fl} pPL2e PactA-cre Phyper-cbpB pPL1 dacA</i> (<i>dacA^{fl} cre-cbpB pdacA</i>)	This study
DP-L7130	<i>dacA^{fl} pPL2e PactA-cre Phyper-cbpB pPL1 disA</i> (<i>dacA^{fl} cre-cbpB pdisA</i>)	This study
DP-L7131	<i>dacA^{fl} pPL2e PactA-cre Phyper-cbpB Sup1</i>	This study
DP-L7132	<i>dacA^{fl} pPL2e PactA-cre Phyper-cbpB Sup2</i>	This study
DP-L7133	<i>dacA^{fl} pPL2e PactA-cre Phyper-cbpB Sup3</i>	This study
DP-L7134	<i>dacA^{fl} pPL2e PactA-cre Phyper-cbpB Sup4</i>	This study
DP-L7135	<i>dacA^{fl} pPL2e PactA-cre Phyper-cbpB Sup5</i>	This study
DP-L7136	<i>dacA^{fl} pPL2e PactA-cre Phyper-cbpB Sup6</i>	This study
DP-L7137	<i>dacA^{fl} pPL2e PactA-cre Phyper-cbpB Sup7</i>	This study
DP-L7138	<i>dacA^{fl} pPL2e PactA-cre Phyper-cbpB Sup8</i>	This study
DP-L7139	<i>dacA^{fl} pPL2e PactA-cre Phyper-cbpB Sup9</i>	This study
DP-L7140	<i>dacA^{fl} pPL2e PactA-cre Phyper-cbpB Sup10</i>	This study
DP-L7141	<i>dacA^{fl} pPL2e PactA-cre Phyper-cbpB Sup11</i>	This study
DP-L7142	<i>dacA^{fl} pPL2e PactA-cre Phyper-cbpB Sup12</i>	This study
DP-L7143	<i>dacA^{fl} pPL2e PactA-cre Phyper-cbpB Sup13</i>	This study
DP-L7144	<i>dacA^{fl} pPL2e PactA-cre Phyper-cbpB Sup14</i>	This study
DP-L7145	<i>dacA^{fl} pPL2e PactA-cre Phyper-cbpB Sup15</i>	This study
DP-L7146	<i>dacA^{fl} pPL2e PactA-cre Phyper-cbpB Sup16</i>	This study
DP-L7147	<i>dacA^{fl} pPL2e PactA-cre Phyper-cbpB Sup17</i>	This study
DP-L7148	<i>dacA^{fl} pPL2e PactA-cre Phyper-cbpB Sup18</i>	This study
DP-L7149	<i>dacA^{fl} pPL2e PactA-cre Phyper-cbpB Sup19</i>	This study

DP-L7150	<i>dacA^{fl} pPL2e PactA-cre Phyper-cbpB Sup20</i>	This study
DP-L7151	<i>dacA^{fl} pPL2e PactA-cre Phyper-cbpB Sup21</i>	This study
DP-L7152	<i>dacA^{fl} pPL2e PactA-cre Phyper-cbpB Sup22</i>	This study
DP-L7153	<i>dacA^{fl} pPL2e PactA-cre Phyper-cbpB Sup23</i>	This study
DP-L7154	<i>dacA^{fl} pPL2e PactA-cre Phyper-cbpB Sup24</i>	This study
DP-L7155	<i>dacA^{fl} pPL2e PactA-cre Phyper-cbpB relAR295S</i>	This study
DP-L6380	<i>ΔdacAΔcbpB</i>	(53)
DP-L6381	<i>ΔdacAΔpstA</i>	(53)
DP-L6542	<i>ΔdacAΔoppB</i>	(53)
DP-L6346	<i>ΔcbpB (Δlmo1009)</i>	(53)
DP-L7156	<i>ΔcbpB + Tn917 from DP-L3903</i>	This study

Table 3.5 Plasmids used in this study

Strain Number	Plasmid	Source
DP-E7157	<i>pPL2e PactA-cre Phyper-cbpB (WT cre-cbpB)</i>	This study
DP-E7158	<i>pPL2e PactA-cre (dacA^{fl} cre)</i>	(56)
DP-E7159	<i>pPL1 dacA</i>	This study
DP-E7160	<i>pPL1 PdacA-disA</i>	This study
DP-E7161	<i>pET20b cbpB-His-SII</i>	This study
DP-E7162	<i>pET20b relA</i>	This study

Chapter 4: Concluding thoughts and future directions

We have uncovered the mode of translational repression for the *hly* gene. The extensive mRNA secondary structure that occludes the RBS changes according to the bacterial growth phase. We did not describe what mechanism underpins the change in mRNA structure. Here I will outline a number of potential hypotheses and ways to test them so that the regulatory mechanism can be elucidated.

As stated in the discussion, there are many differences between growing and non-growing bacteria with respect to macromolecular organization and structure. The sharp reduction in the number of ribosomes in a cell due to stationary phase and the homogenization of the translation networks could indicate a preference for one species of mRNA over another (84). It is believed that 10-15% of the translation in a cell is co-transcriptional, but the vast majority of the translation is co-translational. Interruptions in the transcription-translation, membrane insertions (aka, transertion) network could mean that the proportion of the translation in the cell that is coupled to transcription changed as well. Co-translational transcription has been implicated in the expression of genes with mRNA secondary structures (45). Here, researchers used the T7 promoter to drive transcription of their gene of interest. T7 RNAP is believed to decouple transcription and translation due to its high processivity rate. Attempts to construct such a strain in *L. monocytogenes* were unsuccessful. It also is not known whether the translationally repressed mRNA species occurs during transcription or when the mRNA is mature. The stability of the *hly* transcript is much higher during stationary phase (and during general starvation) than during exponential growth. Since LLO is highly synthesized during stationary phase, understanding why the mRNA half-life increases would be key to determining growth phase dependent expression. Single molecule fluorescent microscopy experiments have been utilized to understand cellular structure during many different environmental conditions. Microfluidic experiments with proper reporter systems could also be important to understanding *L. monocytogenes* during non-growing conditions. The biosafety level of *L. monocytogenes* might be an impediment to implementing these tools, so investigations in *B. subtilis* could be a viable alternative for future studies.

DMS-MaPseq is a powerful tool to understanding RNA structure. One of the curious data points to come from the analysis on live bacteria is the modification of RNA near the RBS beyond what was expected. This could be because the secondary structure forms an opening in the stem to facilitate ribosome binding. Ribosome profiling would be a great tool to understand how ribosomes interact with the *hly* mRNA.

The most limiting factor to further studies of *L. monocytogenes* behavior in the non-growing conditions of the phagosome is that it represents such a fleeting moment in the pathogenic lifecycle. Bacteria must respond quickly to the environmental conditions and stresses of the phagosome and this is challenging for understanding those conditions. Important experiments such as ribosome profiling and DMSMaPseq of bacteria in the phagosome versus the cytosol are technically challenging due to the low recovery of genetic material from infected cells at early time points, as well as the timing for collecting the material. Finding a mutant that produces LLO protein that is defective for vacuolar escape but does not affect expression would be a key requirement for these experiments.

The structure of *hly* is not the only example of such a massive mRNA intramolecular structure (45). It is not known if other transcripts behave this way as well. Identifying other genes from other organisms would help to determine if *hly* is “coded” to behave this way. Though we know that *hly* forms the extensive structure in *B. subtilis*, we do not know if it

behaves in a similar growth phase dependent way. If WT *hly* is secreted as much as a PEST mutant in non-growing conditions in *B. subtilis*, there are probably many other genes that behave similarly. Understanding this mode of regulation would be illuminate how bacteria survive long periods of starvation.

c-di-AMP

c-di-AMP signaling in *L. monocytogenes*, as with other bacteria, is an important aspect of microbiology with implications across the tree of life. Both c-di-AMP and (p)ppGpp are present in multiple domains of life, with many functions that are still unknown. In *Listeria* alone there are confirmed c-di-AMP binding proteins with no known functions. It is possible that similar strategies to the one documented here (over-expression during c-di-AMP deficient conditions) might be fruitful in identifying their functions by screening for phenotypes and identifying suppressor mutations. An outstanding question for the c-di-AMP field in *S. aureus* is how the stringent response is activated during high c-di-AMP levels and if there is a related mechanism to maintain homeostasis of both molecules. It is unclear if organisms that are known to be affected by c-di-AMP in this way respond similarly when the molecule is limiting.

Elucidating how c-di-AMP metabolism is affected during the course of infection and different environmental conditions would provide insight into understanding how bacteria respond to different stresses, and activate host innate immune responses. To date, studies have been hindered due to absence of adequate biosensors that measure c-di-AMP levels dynamically and sensitively. Future work on c-di-AMP in pathogens should focus on the stimuli that affect the related signaling networks and second messenger metabolism.

The discovery of new nucleotide second messenger molecules in diverse clades of bacteria has illuminated the sheer number of possible molecules that exist in nature (50, 51). The functions of all of these molecules and their relationships to one another will be a keen area of interest. It will also be interesting to see how these molecules interact with the mammalian immune system, if at all.

Chapter 5: References

1. A. N. Desai, A. Anyoha, L. C. Madoff, B. Lassmann, Changing epidemiology of *Listeria monocytogenes* outbreaks, sporadic cases, and recalls globally: A review of ProMED reports from 1996 to 2018. *International Journal of Infectious Diseases*. **84**, 48–53 (2019).
2. N. E. Freitag, G. C. Port, M. D. Miner, *Listeria monocytogenes* — from saprophyte to intracellular pathogen. *Nature Publishing Group*. **7**, 623–628 (2009).
3. K. Hoelzer, R. Pouillot, S. Dennis, Animal models of listeriosis: a comparative review of the current state of the art and lessons learned. *Veterinary Research*. **43**, 1–27 (2012).
4. A. S. Cross, What is a virulence factor? *Critical Care*, 1–2 (2015).
5. R. E. Vance, R. R. Isberg, D. A. Portnoy, Patterns of Pathogenesis: Discrimination of Pathogenic and Nonpathogenic Microbes by the Innate Immune System. *Cell Host and Microbe*. **6**, 10–21 (2009).
6. A. Hadjilouka, S. Paramithiotis, E. H. Drosinos, Genetic Analysis of the *Listeria* Pathogenicity Island 1 of *Listeria monocytogenes* 1/2a and 4b Isolates. *Current Microbiology*. **75**, 857–865 (2018).
7. M. L. Reniere, A. T. Whiteley, D. A. Portnoy, An In Vivo Selection Identifies *Listeria monocytogenes* Genes Required to Sense the Intracellular Environment and Activate Virulence Factor Expression, 1–27 (2016).
8. J. A. Vazquez-Boland *et al.*, *Listeria* pathogenesis and molecular virulence determinants. *Clinical Microbiology Reviews*. **14**, 584–640 (2001).
9. L. Tilney, D. A. Portnoy, Actin Filaments and the Growth, Movement, and Spread of the Intracellular Bacterial Parasite. **109**, 1597–1608 (1989).
10. A. R. Witter, B. M. Okunnu, R. E. Berg, The Essential Role of Neutrophils during Infection with the Intracellular Bacterial Pathogen *Listeria monocytogenes*. *J.I.* **197**, 1557–1565 (2016).
11. M. Lecuit, Human listeriosis and animal models. *Microbes and Infection*. **9**, 1216–1225 (2007).
12. A. I. Bakardjiev, B. A. Stacy, D. A. Portnoy, Growth of *Listeria monocytogenes* in the Guinea Pig Placenta and Role of Cell-to-Cell Spread in Fetal Infection. *J INFECT DIS*, 1889–1897 (2005).
13. J.-L. Gaillard, P. Berche, P. Sansonetti, Transposon Mutagenesis as a Tool to Study the Role of Hemolysin in the Virulence of *Listeria monocytogenes*. *Infection and Immunity*. **52**, 50–55 (1986).

14. S. Kathariou, *Listeria monocytogenes* Virulence and Pathogenicity, a Food Safety Perspective. *Journal of Food Protection*, 1811–1829 (2002).
15. A. Le Monnier *et al.*, ActA is required for crossing of the fetoplacental barrier by *Listeria monocytogenes*. *Infection and Immunity*. **75**, 950–957 (2007).
16. W. Li *et al.*, NLRP3 inflammasome activation contributes to *Listeria monocytogenes*-induced animal pregnancy failure. *BMC Veterinary Research*, 1–11 (2016).
17. D. B. McKay, C. Y. Lu, Listeriolysin as a Virulence Factor in *Listeria monocytogenes* Infection of Neonatal Mice and Murine Decidual Tissue. **59**, 4286–4290 (1991).
18. D. A. Portnoy, S. Jacks, D. J. Hinrichs, Role of hemolysin for the intracellular growth of *Listeria monocytogenes*. *Journal of Experimental Medicine*. **167**, 1459–1471 (1988).
19. J.-P. Levrard *et al.*, Real-time observation of *Listeria monocytogenes*-phagocyte interactions in living zebrafish larvae. *Infection and Immunity*. **77**, 3651–3660 (2009).
20. A. L. Decatur, A PEST-Like Sequence in Listeriolysin O Essential for *Listeria monocytogenes* Pathogenicity. *Science*. **290**, 992–995 (2000).
21. S. Jones, D. A. Portnoy, Characterization of *Listeria monocytogenes* Pathogenesis in a Strain Expressing Perfringolysin O in Place of Listeriolysin O. *Infection and Immunity*. **62**, 5608–5613 (1994).
22. D. A. Portnoy, R. K. Tweten, M. Kehoe, J. Bielecki, Capacity of Listeriolysin O, Streptolysin O, and Perfringolysin O To Mediate Growth of *Bacillus subtilis* within Mammalian Cells. *Infection and Immunity*. **60**, 2710–2717 (1992).
23. Z. Wei *et al.*, Characterization of *Listeria monocytogenes* Expressing Anthrolysin O and Phosphatidylinositol-Specific Phospholipase C from *Bacillus anthracis*. *Infection and Immunity*. **73**, 6639–6646 (2005).
24. J. Hardy *et al.*, Extracellular Replication of *Listeria monocytogenes* in the Murine Gall Bladder. *Science*. **303**, 851–853 (2004).
25. G. S. Jones *et al.*, Intracellular *Listeria monocytogenes* comprises a minimal but vital fraction of the intestinal burden following foodborne infection. *Infection and Immunity*. **83**, 3146–3156 (2015).
26. J. T. Roll, C. J. Czuprynski, Hemolysin is required for extraintestinal dissemination of *Listeria monocytogenes* in intragastrically inoculated mice. **58**, 3147–3150 (1990).
27. C. Geoffroy, J.-L. Gaillard, J. E. Alouf, P. Berche, Purification, Characterization, and Toxicity of the Sulfhydryl-Activated Hemolysin Listeriolysin O from *Listeria monocytogenes*. *Infection and Immunity*. **55**, 1641–1646 (1987).

28. I. J. Glomski, M. M. Gedde, A. W. Tsang, J. A. Swanson, D. A. Portnoy, The *Listeria monocytogenes* hemolysin has an acidic pH optimum to compartmentalize activity and prevent damage to infected host cells. *J Cell Biol.* **156**, 1029–1038 (2002).
29. D. W. Schuerch, E. M. Wilson-Kubalek, R. K. Tweeten, Molecular basis of listeriolysin O pH dependence. *Proc. Natl. Acad. Sci. U.S.A.* **102**, 12537–12542 (2005).
30. M.-A. Lety, C. Frehel, P. Berche, A. Charbit, Critical role of the N-terminal residues of listeriolysin O in phagosomal escape and virulence of *Listeria monocytogenes*. *Molecular Microbiology*, 367–379 (2002).
31. S. Koster *et al.*, Crystal structure of listeriolysin O reveals molecular details of oligomerization and pore formation. *Nature Communications.* **5**, 1–14 (2014).
32. M. Rechsteiner, S. Rogers, PEST sequences and regulation by proteolysis. *Trends in Biochemical Sciences.* **21**, 267–271 (1996).
33. S. Rogers, R. Wells, M. Rechsteiner, Amino Acid Sequence Common to Rapidly Degraded Proteins: The PEST Hypothesis. *Science.* **234**, 364–368 (1986).
34. P. Schnupf, D. A. Portnoy, A. L. Decatur, Phosphorylation, ubiquitination and degradation of listeriolysin O in mammalian cells: role of the PEST-like sequence. *Cellular Microbiology.* **8**, 353–364 (2006).
35. P. Schnupf, J. Zhou, A. Varshavsky, D. A. Portnoy, Listeriolysin O Secreted by *Listeria monocytogenes* into the Host Cell Cytosol Is Degraded by the N-End Rule Pathway. *Infection and Immunity.* **75**, 5135–5147 (2007).
36. P. Schnupf *et al.*, Regulated translation of listeriolysin O controls virulence of *Listeria monocytogenes*. *Molecular Microbiology.* **61**, 999–1012 (2006).
37. A. Shen, D. E. Higgins, The 5' untranslated region-mediated enhancement of intracellular listeriolysin O production is required for *Listeria monocytogenes* pathogenicity. *Molecular Microbiology.* **57**, 1460–1473 (2005).
38. F. Crick, Central Dogma of Molecular Biology. *Nature.* **227**, 561–563 (2004).
39. H. M. Johnson, W. M. Barnes, F. G. Chumley, L. Bossi, J. R. Roth, Model for regulation of the histidine operon of *Salmonella*. *Proceedings of the National Academy of Sciences.* **77**, 508–512 (1980).
40. J. L. Chaney, P. L. Clark, Roles for Synonymous Codon Usage in Protein Biogenesis. *Annu. Rev. Biophys.* **44**, 143–166 (2015).
41. R. Grantham, C. Gautier, M. Gouy, Codon frequencies in 119 individual genes confirm consistent choices of degenerate bases according to genome type. *Nucleic Acids Research.* **8**, 1893–1912 (1980).

42. T. F. Clarke, Increased incidence of rare codon clusters at 5' and 3' gene termini: implications for function. *BMC Genomics*, 1–10 (2010).
43. T. Ikemura, Codon Usage and tRNA Content in Unicellular and Multicellular Organisms. *Molecular Biology Evolution*, 13–34 (1985).
44. D. B. Goodman, G. M. Church, S. Kosuri, Causes and Effects of N-Terminal Codon Bias in Bacterial Genes. *Science*. **342**, 475–479 (2013).
45. S. Bhattacharyya *et al.*, Accessibility of the Shine-Dalgarno Sequence Dictates N-Terminal Codon Bias in *E. coli*. *MOLCEL*. **70**, 894–905.e5 (2018).
46. K. Bentele, P. Saffert, R. Rauscher, Z. Ignatova, N. B. U. thgen, Efficient translation initiation dictates codon usage at gene start. *Molecular Systems Biology*. **9**, 1–10 (2013).
47. M. K. Sands, R. B. Roberts, The effects of a tryptophan-histidine deficiency in a mutant of *Escherichia coli*. *Journal of Bacteriology*, 505–511 (1951).
48. G. S. Stent, S. Brenner, A Genetic Locus for the Regulation of Ribonucleic Acid Synthesis. *Proceedings of the National Academy of Sciences*. **47**, 2005–2014 (1961).
49. M. Cashel, J. Gallant, Two Compounds implicated in the Function of the RC Gene of *Escherichia coli*. *Nature*. **221**, 1–4 (1969).
50. A. T. Whiteley *et al.*, Bacterial cGAS-like enzymes synthesize diverse nucleotide signals. *Nature*. **567**, 1–24 (2019).
51. D. Cohen *et al.*, Cyclic GMP–AMP signaling protects bacteria against viral infection. *Nature*, 691–695 (2019).
52. J. J. Woodward, A. T. Iavarone, D. A. Portnoy, c-di-AMP secreted by intracellular *Listeria monocytogenes* activates a host type I interferon response. *Science*. **328**, 1703–1705 (2010).
53. A. T. Whiteley *et al.*, c-di-AMP modulates *Listeria monocytogenes* central metabolism to regulate growth, antibiotic resistance and osmoregulation. *Molecular Microbiology*. **191**, 1–22 (2017).
54. K. Sureka *et al.*, The Cyclic Dinucleotide c-di-AMP Is an Allosteric Regulator of Metabolic Enzyme Function. *Cell Biology*. **158**, 1389–1401 (2014).
55. C. F. Schuster *et al.*, The second messenger c-di-AMP inhibits the osmolyte uptake system OpuC in *Staphylococcus aureus*. *Science Signaling*. **9**, 1–14 (2016).
56. A. T. Whiteley, A. J. Pollock, D. A. Portnoy, The PAMP c-di-AMP Is Essential for *Listeria* Growth in Macrophages and Rich but Not Minimal Media due to a Toxic Increase in (p)ppGpp. *Cell Host and Microbe*. **17**, 788–798 (2015).

57. R. M. Corrigan, L. Bowman, A. R. Willis, V. Kaefer, A. Gründling, Cross-talk between Two Nucleotide-signaling Pathways in *Staphylococcus aureus*. *Journal of Biological Chemistry*. **290**, 5826–5839 (2015).
58. T. N. Huynh *et al.*, An HD-domain phosphodiesterase mediates cooperative hydrolysis of c-di-AMP to affect bacterial growth and virulence. *Proceedings of the National Academy of Sciences*. **112**, E747–E756 (2015).
59. F. M. Commichau, J. L. Heidemann, R. Ficner, J. Stülke, Making and Breaking of an Essential Poison: the Cyclases and Phosphodiesterases That Produce and Degrade the Essential Second Messenger Cyclic di-AMP in Bacteria. *Journal of Bacteriology*. **201**, 562–14 (2019).
60. T. N. Huynh *et al.*, Cyclic di-AMP targets the cystathionine beta-synthase domain of the osmolyte transporter OpuC. *Molecular Microbiology*. **102**, 233–243 (2016).
61. P. H. Choi, K. Sureka, J. J. Woodward, L. Tong, Molecular basis for the recognition of cyclic-di-AMP by PstA, a PII -like signal transduction protein. *MicrobiologyOpen* (2015), doi:10.1002/mbo3.243.
62. F. Gruswitz, J. O'Connell III, R. M. Stroud, Inhibitory complex of the transmembrane ammonia channel, AmtB, and the cytosolic regulatory protein, GlnK, at 1.96 Å. *Proceedings of the National Academy of Sciences*, 42–47 (2007).
63. M. J. Conroy *et al.*, The crystal structure of the *Escherichia coli* AmtB–GlnK complex reveals how GlnK regulates the ammonia channel. *Proceedings of the National Academy of Sciences*, 1213–1218 (2007).
64. N. F. Kamaruzzaman, S. Kendall, L. Good, Targeting the hard to reach: challenges and novel strategies in the treatment of intracellular bacterial infections. *British Journal of Pharmacology*. **174**, 2225–2236 (2016).
65. L. Radoshevich, P. Cossart, *Listeria monocytogenes*: towards a complete picture of its physiology and pathogenesis. *Nat Rev Micro*. **16**, 32–46 (2017).
66. R. K. Tweten, Cholesterol-Dependent Cytolysins, a Family of Versatile Pore-Forming Toxins. *Infection and Immunity*. **73**, 6199–6209 (2005).
67. R. Gilbert, G. Anderluh, J. Lakey, Eds. (Advances in Experimental Medicine and Biology, 2010), pp. 1–189.
68. P. Schnupf *et al.*, Regulated translation of listeriolysin O controls virulence of *Listeria monocytogenes*. *Molecular Microbiology*. **61**, 999–1012 (2006).
69. P. M. Sharp, W.-H. Li, The codon adaptation index - a measure of directional synonymous codon usage bias, and its potential applications. *Nucleic Acids Research*, 1–15 (1987).

70. A. Grote *et al.*, JCat: a novel tool to adapt codon usage of a target gene to its potential expression host. *Nucleic Acids Research*. **33**, W526–W531 (2005).
71. P. Lauer, M. Y. N. Chow, M. J. Loessner, D. A. Portnoy, R. Calendar, Construction, Characterization, and Use of Two *Listeria monocytogenes* Site-Specific Phage Integration Vectors. *Journal of Bacteriology*. **184**, 4177–4186 (2002).
72. F. Eggenhofer, H. Tafer, P. F. Stadler, I. L. Hofacker, RNApredator: fast accessibility-based prediction of sRNA targets. *Nucleic Acids Research*. **39**, W149–W154 (2011).
73. R. Lorenz *et al.*, ViennaRNA Package 2.0. *Algorithms Mol Biol*. **6**, 751–31 (2011).
74. G. Kudla, A. W. Murray, D. Tollervey, J. B. Plotkin, Coding-Sequence Determinants of Gene Expression in *Escherichia coli*. *Science*. **324**, 252–255 (2009).
75. E. G. Pamer, J. T. Harty, M. J. Bevan, Precise prediction of a dominant class I MHC-restricted epitope of *Listeria monocytogenes*. *Nature*. **353**, 852–855 (1991).
76. K. S. Bahjat *et al.*, Cytosolic entry controls CD8⁺-T-cell potency during bacterial infection. *Infection and Immunity*. **74**, 6387–6397 (2006).
77. J. Johansson *et al.*, An RNA Thermosensor Controls Expression of Virulence Genes in. *Cell Biology*. **110**, 551–561 (2002).
78. M. H. de Smit, J. van Duin, Secondary structure of the ribosome binding site determines translational efficiency: A quantitative analysis. *Proceedings of the National Academy of Sciences*. **87**, 7668–7672 (1990).
79. G. Nilsson, J. G. Berlasco, S. N. Cohen, A. von Gabain, Growth-rate dependent regulation of mRNA stability in *Escherichia coli*. *Nature*. **312**, 75–77 (1984).
80. S. A. Emory, J. G. Belasco, The ompA 5' Untranslated RNA Segment Functions in *Escherichia coli* as a Growth-Rate-Regulated mRNA Stabilizer Whose Activity Is Unrelated to Translational Efficiency. *Journal of Bacteriology*. **172**, 4472–4481 (1990).
81. K. Potrykus, M. Cashel, (p)ppGpp: Still Magical? *Annu. Rev. Microbiol*. **62**, 35–51 (2008).
82. C. A. Reeve, P. S. Amy, A. Martin, Role of Protein Synthesis in the Survival of Carbon-Starved *Escherichia coli* K-12. *Journal of Bacteriology*. **160**, 1041–1046 (1984).
83. O. Gefen, O. Fridman, I. Ronin, N. Q. Balaban, Direct observation of single stationary-phase bacteria reveals a surprisingly long period of constant protein production activity. *Proceedings of the National Academy of Sciences*. **111**, 556–561 (2014).
84. S. Bakshi, H. Choi, J. C. Weisshaar, The spatial biology of transcription and translation in rapidly growing *Escherichia coli*. *Front. Microbiol*. **6**, 1–15 (2015).

85. P. J. Lewis, S. D. Thaker, J. Errington, Compartmentalization of transcription and translation in *Bacillus subtilis*. *The EMBO Journal*. **19**, 710–718 (2000).
86. S. W. Artz, J. R. Broach, Histidine regulation in *Salmonella typhimurium*: An activator-attenuator model of gene expression. *Proceedings of the National Academy of Sciences*. **72**, 3453–3457 (1975).
87. J.-D. Sauer *et al.*, Short Article. *Cell Host and Microbe*, 1–8 (2010).
88. D. K. Bishop, D. J. Hinrichs, Adoptive transfer of immunity to *Listeria monocytogenes*. The influence of in vitro stimulation on lymphocyte subset requirements. *J.I.*, 2005–2009 (1987).
89. M. Cashel, J. Gallant, Two Compounds implicated in the Function of the RC Gene of *Escherichia coli*. *Nature*. **221**, 838–841 (1969).
90. K. Liu, A. N. Bittner, J. D. Wang, Diversity in (p)ppGpp metabolism and effectors. *Current Opinion in Microbiology*. **24**, 72–79 (2015).
91. J.-W. Lee, Y.-H. Park, Y.-J. Seok, Rsd balances (p)ppGpp level by stimulating the hydrolase activity of SpoT during carbon source downshift in *Escherichia coli*. *Proc. Natl. Acad. Sci. U.S.A.* **115**, E6845–E6854 (2018).
92. M. Fang, C. E. Bauer, Regulation of stringent factor by branched-chain amino acids. *Proceedings of the National Academy of Sciences*. **115**, 6446–6451 (2018).
93. A. Battesti, E. Bouveret, Acyl carrier protein/SpoT interaction, the switch linking SpoT-dependent stress response to fatty acid metabolism. *Molecular Microbiology*. **62**, 1048–1063 (2006).
94. C. E. Witte *et al.*, Cyclic di-AMP is critical for *Listeria monocytogenes* growth, cell wall homeostasis, and establishment of infection. *mBio*. **4**, e00282–13 (2013).
95. J.-D. Sauer *et al.*, *Listeria monocytogenes* Triggers AIM2-Mediated Pyroptosis upon Infrequent Bacteriolysis in the Macrophage Cytosol. *Cell Host and Microbe*. **7**, 412–419 (2010).
96. S. Ronneau *et al.*, Regulation of (p)ppGpp hydrolysis by a conserved archetypal regulatory domain. *Nucleic Acids Research*. **47**, 843–854 (2018).
97. F. Rao, Q. Ji, I. Soehano, Z.-X. Liang, Unusual heme-binding PAS domain from YybT family proteins. *Journal of Bacteriology*. **193**, 1543–1551 (2011).
98. A. L. Sonenshein, Control of key metabolic intersections in *Bacillus subtilis*. *Nat Rev Micro*. **5**, 917–927 (2007).

99. M. Mittal, S. Picossi, A. L. Sonenshein, CcpC-Dependent Regulation of Citrate Synthase Gene Expression in *Listeria monocytogenes*. *Journal of Bacteriology*. **191**, 862–872 (2009).
100. H. J. Kim, M. Mittal, A. L. Sonenshein, CcpC-Dependent Regulation of citB and lmo0847 in *Listeria monocytogenes*. *Journal of Bacteriology*. **188**, 179–190 (2005).
101. H. J. Kim, C. Jourlin-Castelli, S.-I. Kim, A. L. Sonenshein, Regulation of the *Bacillus subtilis* ccpC gene by CcpA and CcpC. *Molecular Microbiology*. **43**, 399–410 (2002).
102. T. Hartmann *et al.*, Catabolite Control Protein E (CcpE) Is a LysR-type Transcriptional Regulator of Tricarboxylic Acid Cycle Activity in *Staphylococcus aureus*. *Journal of Biological Chemistry*. **288**, 36116–36128 (2013).
103. Y. Ding *et al.*, Metabolic sensor governing bacterial virulence in *Staphylococcus aureus*. *Proceedings of the National Academy of Sciences*. **111**, E4981–E4990 (2014).
104. J. L. Portman, S. B. Dubensky, B. N. Peterson, A. T. Whiteley, D. A. Portnoy, Activation of the *Listeria monocytogenes* Virulence Program by a Reducing Environment. *mBio*. **8**, 7–13 (2017).
105. C. M. Taylor *et al.*, *Listeria monocytogenes* relA and hpt mutants are impaired in surface-attached growth and virulence. *Journal of Bacteriology*. **184**, 621–628 (2002).
106. Z. Otwinoski, W. Minor, Processing of X-Ray Diffraction Data Collected in Oscillation Mode. *Method in Enzymology*. **276**, 307–326 (1997).
107. P. D. Adams *et al.*, PHENIX: building new software for automated crystallographic structure determination. *Acta Cryst (2002)*. *D58*, 1948–1954 [doi:10.1107/S0907444902016657], 1948–1954 (2002).
108. P. Emsley, K. Cowtan, Coot: model-building tools for molecular graphics. *Acta Cryst (2004)*. *D60*, 2126–2132 [doi:10.1107/S0907444904019158], 2126–2132 (2004).